J. Fluid Mech. (2003), *vol.* 487, *pp.* 1–42. © 2003 Cambridge University Press
DOI: 10.1017/S0022112003004816 Printed in the United Kingdom

Resonant three-dimensional nonlinear sloshing in a square-base basin

By ODD M. FALTINSEN[1], OLAV F. ROGNEBAKKE[2] AND ALEXANDER N. TIMOKHA[3]

[1]Department of Marine Technology, NTNU, N-7491 Trondheim, Norway

[2]MARINTEK, P.O. Box 4125, N-7450 Trondheim, Norway

[3]Institute of Mathematics, National Academy of Sciences of Ukraine, Tereschenkivska, 3 str., Kiev, 01601, Ukraine

(Received 29 August 2002 and in revised form 20 December 2002)

An asymptotic modal system is derived for modelling nonlinear sloshing in a rectangular tank with similar width and breadth. The system couples nonlinearly nine modal functions describing the time evolution of the natural modes. Two primary modes are assumed to be dominant. The system is equivalent to the model by Faltinsen *et al.* (2000) for the two-dimensional case. It is validated for resonant sloshing in a square-base basin. Emphasis is on finite fluid depth but the behaviour with decreasing depth to intermediate depths is also discussed. The tank is forced in surge/sway/roll/pitch with frequency close to the lowest degenerate natural frequency. The theoretical part concentrates on periodic solutions of the modal system (steady-state wave motions) for longitudinal (along the walls) and diagonal (in the vertical diagonal plane) excitations. Three types of solutions are established for each case: (i) 'planar'/'diagonal' resonant standing waves for longitudinal/diagonal forcing, (ii) 'swirling' waves moving along tank walls clockwise or counterclockwise and (iii) 'square'-like resonant standing wave coupling in-phase oscillations of both the lowest modes. The frequency domains for stable and unstable waves (i)–(iii), the contribution of higher modes and the influence of decreasing fluid depth are studied in detail. The zones where either unstable steady regimes exist or there are two or more stable periodic solutions with similar amplitudes are found. New experimental results are presented and show generally good agreement with theoretical data on effective domains of steady-state sloshing. Three-dimensional sloshing regimes demonstrate a significant contribution of higher modes in steady-state and transient flows.

1. Introduction

Two-dimensional resonant fluid sloshing in a rectangular tank has been extensively studied theoretically, experimentally and numerically. This is commonly used to assess sloshing effects in ship tanks. However, a two-dimensional model becomes questionable when the length and the breadth of the tank are of the same order of magnitude, or, in particular, equal. Even if the horizontal excitation is parallel to the walls, a strong three-dimensional flow including chaotic behaviour may occur for resonant excitation at the lowest natural frequency. This is associated with instability of two-dimensional motions relative to spatial disturbances. A similar problem with two conjugate modes occurs for vertical circular cylindrical and spherical tanks.

https://doi.org/10.1017/S0022112003004816 Published online by Cambridge University Press

Fundamental theoretical and experimental work on axial-symmetric tanks have been motivated by the space industry (Abramson 1966 and Mikishev 1978). Theoretical studies of nonlinear sloshing in axial-symmetric tanks are presented by Narimanov, Dokuchaev & Lukovsky (1977), Miles (1984*a*, *b*), Lukovsky (1990) and many others. These studies made significant progress in the theoretical treatment of 'swirling' (rotary) waves due to sway/pitch resonant forcing, which can cause significant longitudinal and transverse horizontal forces. (Abramson *et al.* 1974 demonstrated this experimentally for a spherical LNG tank when the horizontal excitation amplitude is sufficiently large and the excitation amplitude is higher than the lowest natural frequency.)

Stolbetsov (1967) may have been the first to study theoretically nonlinear resonant sloshing in a near-square basin due to horizontal harmonic forcing along one of the walls with excitation frequency close to the lowest natural frequency. He used the perturbation technique by Narimanov (1957) and postulated two types of steady-state solutions. The first one describes two-dimensional steady-state motions ('planar'† waves). The second is equivalent to 'swirling' waves for rectangular geometry. Unfortunately, this original work (as remarked by Lukovsky 1990) contains arithmetic errors. This might be the reason why it did not initiate more detailed studies by other authors. Being familiar with both former Soviet and Western literature, the present authors could find only a limited set of experimental and theoretical works closely related to this topic in the period from 1960 to 1990. Existing theoretical papers on nonlinear sloshing in a square basin are almost always devoted to either Faraday waves (the most cited representative papers and reviews are for instance by Nevolin 1984; Feng & Sethna 1989; Simonelli & Gollub 1989; Henderson & Miles 1990; Nagata 1991; Miles 1994; Perlin & Schultz 2000), free waves in a basin (see some important results by Bridges 1985, 1987; Bryant & Stiassnie 1994, 1995) or wavemaker studies (see the review by Tsai, Yue & Yip 1990).

Since free waves in a basin may be treated as a limiting case of resonant waves with extremely small (zero) excitation amplitude, the papers on this subject are relevant for our study. Bridges (1987) and Bryant & Stiassnie (1994, 1995) presented theoretical results on free nonlinear periodic waves in square tanks of deep and shallow fluid depths. The analysis by Bridges (1987) was restricted to lowest order modes, while Bryant & Stiassnie (1995) used both the third-order Zakharov equation and direct numerical calculations for the original free boundary problem (for infinite depth).

Along with some special periodic solutions described by Bryant & Stiassnie (1994) (which are probably not realized for resonant sloshing) three types of free nonlinear monoharmonical waves can be classified for a square-base basin: (i) 'planar' (two-dimensional) Stokes standing wave, (ii) the standing wave consisting of an oscillation from one corner to the opposite corner with much less motion in other corners (we will call them (following Miles 1994) 'diagonal' or 'square'-like waves) and (iii) 'swirling' waves, where an almost flat crest travels around each of the four sides with an almost flat trough on the opposite side. Bryant & Stiassnie (1995) showed, in particular, that two-dimensional Stokes-type periodic waves are unstable when subjected to three-dimensional perturbations, while three-dimensional waves are stable. Waterhouse (1995) and Ockendon, Ockendon & Waterhouse (1996) studied longitudinally excited

† We follow Miles (1984*b*) and adopt terminology usually used for sloshing in vertical circular cylindrical tanks and in the mechanics of a spherical pendulum.

https://doi.org/10.1017/S0022112003004816 Published online by Cambridge University Press

steady-state multi-mode nonlinear resonance in a near-square tank with either fairly deep or shallow fluid depth. The same three types of waves mentioned above are part of their analysis. Emphasis was on the effect of wall imperfections (Bridges 1985, 1986, 1987 examined earlier the effect of a perturbed square shape on the free waves). Stability of steady-state sway/surge/roll/pitch forced motions and changing from deep or finite to smaller depths with consequent activation of higher modes were not investigated. (This was recently done by Faltinsen *et al.* 2000 and Faltinsen & Timokha 2001, 2002*a* for two-dimensional nonlinear resonant waves.) In addition, there is a need for physical clarification of what can happen for more general types of horizontal/angular excitation, in particular, for diagonal excitation, which has been experimentally investigated by Chen & Arai (1995).

The majority of analytical approaches to nonlinear resonant sloshing in rectangular/circular-base tanks reduce the analysis to governing the equations describing the evolution of asymptotically dominating modes. The most popular method is to use Moiseyev detuning to derive a small-dimensional Hamiltonian systems coupling slowly varying amplitudes of these leading modes. Examples and a general theory of such a class of Hamiltonian systems for free and harmonically forced sloshing are presented in applied mathematical works by Miles (1984*a*, *b*), Bridges (1986, 1988), Feng & Sethna (1989), Nagata (1991), Miles (1994) and many others. They establish multiple steady-state solutions for a given excitation frequency. Since these solutions co-exist, it is not clear which of them will be realized for coupled sloshing and ship motions externally excited by a seaway. Another problem of these analytical methods is the computation of the wave response for small but realistic forcing and intermediate depth/breadth ratio h. Even relative small deviations of excitation frequency may then change the set of leading modes (Faltinsen & Timokha 2001). Alternatives are to use either CFD or a multimodal method.

Examples related to CFD simulations of three-dimensional flows in ship tanks are given by Arai *et al.* (1992*b*), Arai, Cheng & Inoue (1992*a*, 1993), ISSC Report (1997), Faltinsen & Rognebakke (2000) and Wu, Ma & Taylor (1998). Many papers give successful examples for two-dimensional sloshing (see, for instance, recent papers by Celebi & Akyildiz 2002; Sames, Marcouly & Schellin 2002; Aliabadi, Johnson & Abedi 2003). Advantages and disadvantages of various CFD methods are compared in reviews in the ISSC Report (1997) and Ibrahim, Pilipchuk & Ikeda (2001). Reviews by Solaas (1995), Faltinsen & Rognebakke (2000), Faltinsen & Timokha (2002*a*) and Ibrahim *et al.* (2001) provide interested readers with a comparison between several analytical and numerical methods.

We develop in this paper a multimodal approach to nonlinear sloshing in a square-base tank. Its fundamental idea comes from Narimanov (1957) and consists in the derivation of a multi-dimensional system of ordinary differential equations coupling the actual time-evolution of multiple natural modes, where the coefficients are given functions of the fluid depth. A short historical review of the modal methods is given by Faltinsen *et al.* (2000) and Faltinsen & Timokha (2002*a*). Recent studies by La Rocca, Mele & Armenio (1997), Faltinsen & Timokha (2001) and Rognebakke & Faltinsen (2003) demonstrated that this modal method may be adopted for both analytical studies of resonant waves and simulations of coupled 'body–fluid' motions. Lukovsky (1990) showed that the Hamiltonian dynamic system mentioned above can be easily derived from the corresponding modal systems by introducing an additional slowly varying time scale. The modal methods allow any physically possible initial conditions and are in general numerically robust and very time efficient compared to CFD simulations. This makes it realistic to obtain a statistical distribution of the

https://doi.org/10.1017/S0022112003004816 Published online by Cambridge University Press

response variables of sloshing in a ship tank in a stochastic sea. Along with a modal system adopting Moiseyev-like ordering, Faltinsen & Timokha (2001, 2002*a*) presented an adaptive modal modelling technique for two-dimensional waves accounting for dynamic changes in the leading modes (ordering). This method is applicable for both large-amplitude sloshing and intermediate depths. Disadvantages are that the multimodal methods are at present limited to vertical cylindrical tank shapes and two-dimensional rectangular tanks with no roof impact or overturning waves. Further, the free surface should intersect the tank wall perpendicularly and therefore significant run-up at the walls cannot be captured.

Section 2.2 starts with the general modal system derived by Faltinsen *et al.* (2000) as a full analogy of the original free boundary problem for sloshing of a perfect incompressible fluid in irrotational motion. This equivalence was proved by assuming that the free surface allows the usual presentation $z = f(x, y, t)$. It adopts solutions of the spectral problem of linear sloshing as a Fourier basis for the equations of the free surface and the velocity potential. Ordering the external combined sway/surge/pitch/roll forcing as having the highest asymptotic order $O(\epsilon) \ll 1$ we derive in § 2.3 a third-order modal theory in terms of the Fourier coefficients $\beta_{i,j}(t)$ representing the time-evolution of the free surface. This operation assumes that all modes may have dominant behaviour $O(\epsilon^{1/3})$. It is fully consistent with analogous derivations of the adaptive modal system by Faltinsen & Timokha (2001) for two-dimensional flows and with the third-order theory by Zakharov (1968).

In § 3.1 we concentrate on the finite depth ordering, which suggests only two dominant modes associated with the two lowest two-dimensional standing waves occurring along the Ox- and Oy- axes parallel to two orthogonal tank walls. Such ordering is relevant for the case of direct resonant excitation of these modes when corresponding natural frequencies are equal. This may happen for near-square cross-section. The adaptive modal system has then a finite-dimensional nonlinear kernel subsystem of nine ordinary differential equations. Other modal equations are linear. Solutions of this modal system may be studied either analytically or numerically. The system can also be incorporated in the equations of 'body–fluid' motions and provide efficient calculations of the coupled motions.

The modal systems have already been used in practical applications for two-dimensional flows in a ship tank excited by a stochastic sea with many frequency components. Validation of the modal systems is typically done for resonant harmonic excitation of the lowest modes. This makes it possible to establish lower/upper bounds in terms of the excitation frequency domain, fluid depths and excitation amplitude. The particular case of the modal theory from § 3.1 describing two-dimensional sloshing was presented by Faltinsen *et al.* (2000). Systematic comparison of the experimental data and corresponding theoretical results established its qualitative applicability (for extremely small resonant forcing) for $0.24 \lesssim h$, where h is fluid depth. Quantitative agreement can be achieved only for $0.27 \lesssim h$. The failure is caused by the increasing contribution from the higher (non-leading) modes.

In § 3.2–3.3 we examine the resonant sloshing analytically and obtain periodic (steady-state) solutions of the modal system up to $O(\epsilon)$. The procedure combines Bubnov–Galerkin and asymptotic techniques (Faltinsen *et al.* 2000). The secular system of algebraic equations couples the primary amplitudes of the dominating modes. It contains three coefficients, m_1, m_2 and m_3, depending on the depth and the excitation frequency. The properties of solutions depend strongly on the values of m_i. The coefficients are either approximately constant or vary slowly for $h \geqslant 0.337..$ When the depth becomes smaller, solutions of this system undergo strong changes.

https://doi.org/10.1017/S0022112003004816 Published online by Cambridge University Press

The system may even become insoluble for some critical depths. Starting from this system we can derive a Hamiltonian system (of two degrees of freedom) governing the slow-time evolution of the primary amplitudes as in the papers already mentioned. The only difference is that coefficients of that Hamiltonian system are not constant but functions of the excitation frequency (Moiseyev detuning).

The analysis of the secular system for longitudinal excitations (§ 3.4) establishes three, and only three, types of periodic solutions. These are (i) two-dimensional resonant waves (Faltinsen *et al.* 2000), (ii) so-called 'square'-like waves and (iii) 'swirling' waves. The frequency domains where these are stable change with depth. So, for larger finite depths stable 'swirling' motions are realized in the close vicinity of the main resonance, while stable 'planar' waves occur for frequencies not too close to the main resonance. In addition, there is a frequency domain where no stable steady-state solutions exist and, therefore, chaotic wave motions are expected. 'Square'-like waves for large fluid depths either co-exist with 'planar' motions or have a very narrow non-overlapped frequency domain. Initial or transient perturbations will influence which of these waves ('planar' or 'square'-like) will occur in the range where they co-exist. Since it is most probable that zero initial conditions and constant excitation frequency (typical for our experiments) lead to steady-state solutions having the lowest amplitude, 'square'-like waves are not realized in the major part of the experimental series. Since the frequency domain of 'square'-like waves for smaller depths occupies a wide zone near the main resonance and the wave amplitude is lower than for corresponding 'planar' waves, 'square'-lie waves then become of primary interest. Intuitively, this type of wave motion should turn into diagonal-like wave-trains as described by Ockendon *et al.* (1996) for shallow depths. This was established numerically by Wu *et al.* (1998) and observed experimentally by Tomawa & Sueoka (1989).

The experimental studies by Arai *et al.* (1992*a*, *b*, 1993) and Chen & Arai (1995) motivated us to examine steady-state sloshing due to excitation in a diagonal plane (§ 3.5). Three, and only three, types of periodic waves were found. Along with 'swirling' wave motions and a mixed 'square'-like standing wave (the last one always becomes unstable), the analysis establishes the 'diagonal' standing resonant wave. The analysis shows that stable steady-state solutions occur for all frequencies in the vicinity of the main resonance and that there are some frequency domains where two stable standing wave types co-exist.

New model tests results are also presented and compared with the theoretical predictions in §§ 4.1–4.3. Good agreement between predicted and observed types of wave motions in different frequency domains was found. The experiments confirmed the existence of three-dimensional wave motions predicted theoretically (see figure 1 demonstrating experimental observations of 'swirling' phenomena). Although we did not focus on the influence of the excitation amplitude on wave amplitude response, both the theory and isolated experimental series showed that the frequency domains of the three-dimensional response increases with increasing forcing. The numerical results for the three-dimensional wave amplitudes near the walls may in many cases give lower values than the measured ones. The relative errors of our asymptotic model are between 7% and 30% in the presented cases. The discrepancy for predictions by leading modes is up to 200%. This confirms a significant contribution of the higher modes and indicates a possible further modification of the modal systems to account for secondary resonance in a similar way as done by Faltinsen & Timokha (2001) for two-dimensional sloshing. Additional improvements of the theory consist of a matching with local near-wall phenomena.

https://doi.org/10.1017/S0022112003004816 Published online by Cambridge University Press

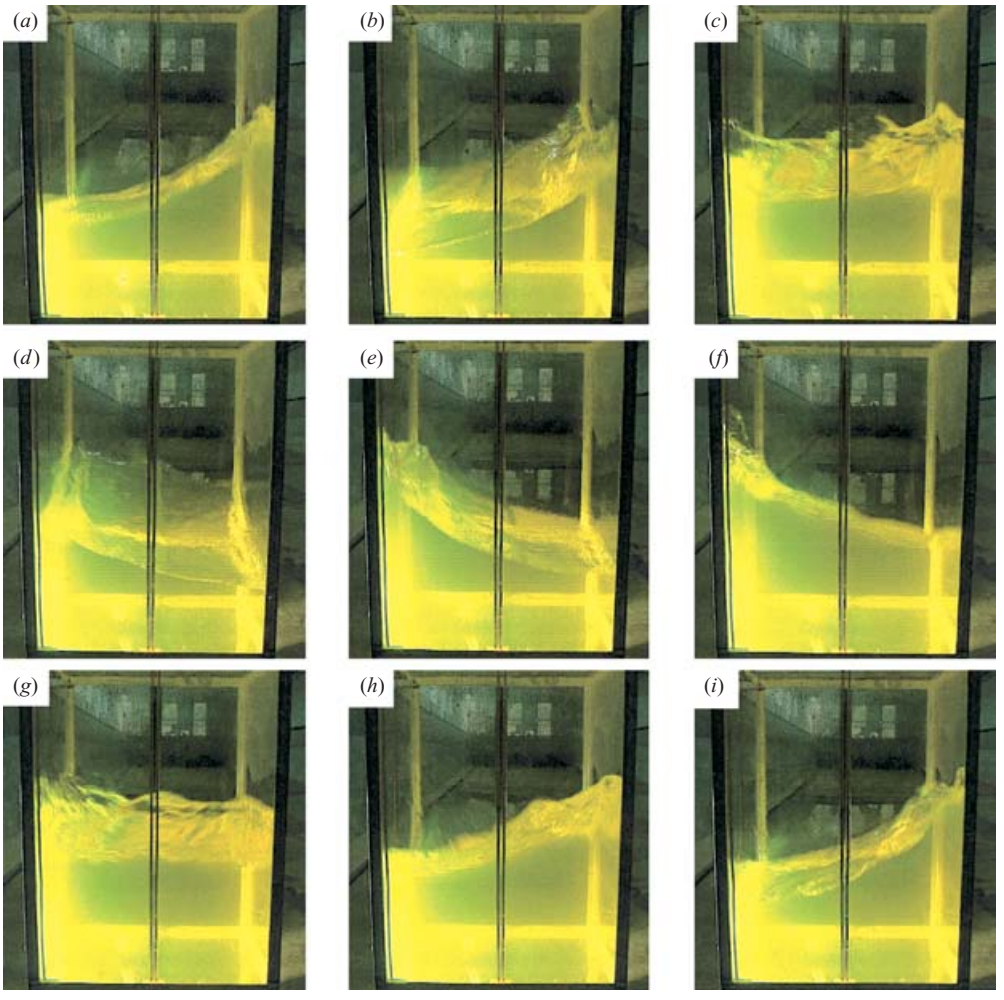


FIGURE 1. Photo time series (from (*a*) to (*i*)) demonstrating counterclockwise (top view) 'swirling' wave motions in a square-base tank for the depth/breadth ratio $h = 0.508$. The tank is excited longitudinally (back and forth motions relative to the camera) with amplitude/breadth ratio $H = 0.0078$. The excitation frequency is equal to the lowest natural frequency.

2. Statement of the problem

2.1. *Geometric preliminaries and free boundary problem*

Let a rigid open parallelepipedal tank with breadth L_1, width L_2 and height D be partially filled by a perfect fluid with the mean depth h. We assume potential flow and make lengths non-dimensional by dividing with L_1, so that we consider a tank with breadth 1, width $1/r = L_2/L_1$ and height D/L_1. Thus new values of the physical constants $h := h/L_1$, $g := g/L_1$ (g is the gravitational acceleration) etc. are defined. This means that h in the following text is dimensionless and g has dimension $[s^{-2}]$. Since the analysis assumes no roof impact, D is not a parameter in our studies.

The motions of the tank are described by a pair of time-dependent vectors $\boldsymbol{v}_O(t)$ and $\boldsymbol{\omega}(t) = \dot{\boldsymbol{\psi}}(t)$ representing instantaneous translatory and angular velocities of the mobile Cartesian coordinate system $Oxyz$ relative to an absolute coordinate system

https://doi.org/10.1017/S0022112003004816 Published online by Cambridge University Press

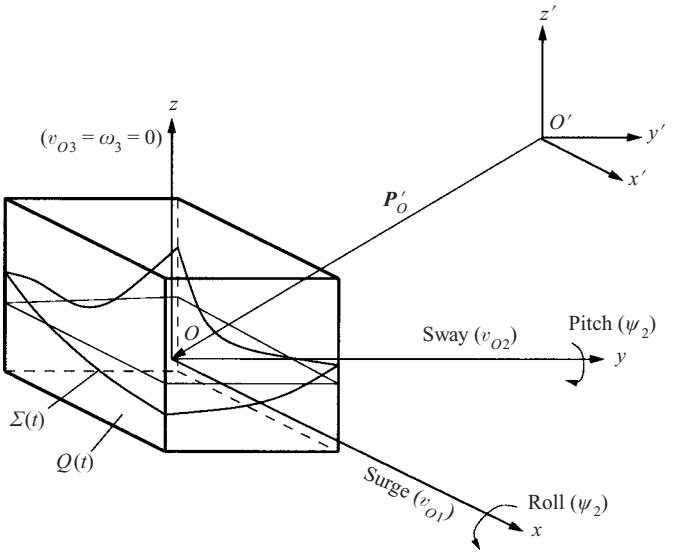


FIGURE 2. Sketch of the tank moving in space. The vectors $\boldsymbol{P}'_O, \boldsymbol{\omega} = (\omega_1, \omega_2, \omega_3)$ and $\boldsymbol{v}_O = (v_{O1}, v_{O2}, v_{O3})$ are considered in the moving coordinate system $Oxyz$ fixed to the rigid tank.

$O'x'y'z'$ (figure 2). The coordinate system $Oxyz$ is rigidly fixed to the tank. Its origin O coincides with the middle point of the mean fluid surface so that the mean fluid surface belongs to the Oxy-plane and the Ox and Oy-axes are parallel to the vertical walls. Since any absolute position vector $\boldsymbol{P}'(t) = (x', y', z')$ can be decomposed into the sum of $\boldsymbol{P}'_O(t) = \vec{O'O}$ and the relative position vector $\boldsymbol{P} = (x, y, z)$, the gravity potential U depends on the spatial coordinates (x, y, z) and time t, namely $U(x, y, z, t) = -\boldsymbol{g} \cdot \boldsymbol{P}'$, $\boldsymbol{P}' = \boldsymbol{P}'_O + \boldsymbol{P}$, where $\boldsymbol{g}$ is the gravitational acceleration vector. The derivation of the corresponding hydrodynamic free boundary problem is given in many textbooks (see, for instance, Moiseyev & Rumyantsev 1968 and Narimanov *et al.* 1977). When $\boldsymbol{v}_O(t)$ and $\boldsymbol{\omega}(t)$ (or $\boldsymbol{\psi}(t)$) are given functions (prescribed motions of the tank), this problem takes the following form:

$$\left.\begin{aligned} &\Delta\Phi = 0 \quad \text{in } Q(t), \ \frac{\partial\Phi}{\partial\nu} = \boldsymbol{v}_O \cdot \boldsymbol{\nu} + \boldsymbol{\omega} \cdot [\boldsymbol{P} \times \boldsymbol{\nu}] \quad \text{on } S(t), \\ &\frac{\partial\Phi}{\partial\nu} = \boldsymbol{v}_O \cdot \boldsymbol{\nu} + \boldsymbol{\omega} \cdot [\boldsymbol{P} \times \boldsymbol{\nu}] - \frac{\xi_t}{|\nabla\xi|} \quad \text{on } \Sigma(t), \quad \int_{Q(t)} \mathrm{d}Q = \text{const}, \\ &\frac{\partial\Phi}{\partial t} + \tfrac{1}{2}(\nabla\Phi)^2 - \nabla\Phi \cdot (\boldsymbol{v}_O + \boldsymbol{\omega} \times \boldsymbol{P}) + U = 0 \quad \text{on } \Sigma(t). \end{aligned}\right\} \tag{2.1}$$

Here the unknowns are the function $\xi(x, y, z, t)$ defining the free-surface evolution $\Sigma(t) : \xi(x, y, z, t) = 0$ and the absolute velocity potential $\Phi(x, y, z, t)$ which should be calculated in a time-varying volume $Q(t)$ confined to the wetted body surface $S(t)$ and $\Sigma(t)$; $\boldsymbol{\nu}$ is the outward normal to $Q(t)$. The evolutional free boundary problem (2.1) should be completed by either initial or periodicity conditions. The initial (Cauchy) conditions require

$$\xi(t_0, x, y, z) = \xi_0(x, y, z), \quad \left.\frac{\partial\Phi}{\partial\nu}\right|_{\Sigma(t_0)} = \Phi_0(x, y, z) \tag{2.2}$$

https://doi.org/10.1017/S0022112003004816 Published online by Cambridge University Press

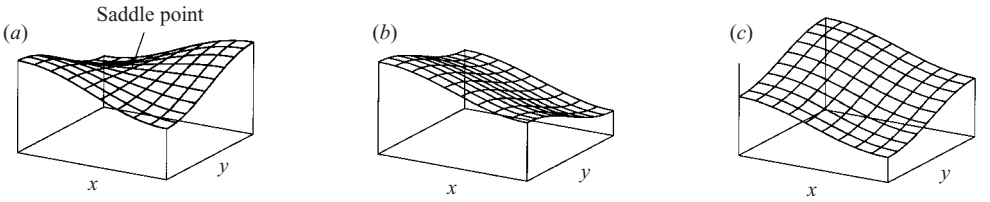


FIGURE 3. Sketches of three-dimensional wave patterns associated with modal shapes (2.6) and (2.7). Here (*a*) illustrates the shape of (2.6), but 'squares' $S_2^1(x, y)$ and $S_1^1(x, y)$ of (2.7) are shown in (*b*) and (*c*) respectively.

to be known at $t = t_0$. The periodicity conditions are in many applied problems associated with periodicity of the wave pattern and velocity field, i.e.

$$\xi(t + T, x, y, z) = \xi(t, x, y, z), \quad \nabla\Phi(t + T, x, y, z) = \nabla\Phi(t, x, y, z). \tag{2.3}$$

This requires that $Q(t+T) = Q(t)$. Further, the last equality in (2.3) is justified by the first one (for ξ) establishing the equivalence of instantaneous fluid shapes at t and $t + T$.

2.2. *Natural modes and modal system by Faltinsen et al. (2000)*

When $\boldsymbol{v}_O = \boldsymbol{\omega} = \mathbf{0}$, the linearization of equation (2.1) describes natural waves $\Phi = \exp(\mathrm{i}\sigma_{i,j}t)\varphi_{i,j}(x, y, z)$, ($\mathrm{i}^2 = -1$), where

$$\left.\begin{aligned} &\varphi_{i,j}(x, y, z) = f_i^{(1)} f_j^{(2)} \tfrac{\cosh(\lambda_{i,j}(z+h))}{\cosh(\lambda_{i,j}h)}, \\ &\lambda_{i,j} = \pi\sqrt{i^2 + r^2 j^2}, \quad \sigma_{i,j}^2 = g\lambda_{i,j}\tanh(\lambda_{i,j}h), \end{aligned}\right\} i, j \geqslant 0, \quad i + j \neq 0, \tag{2.4}$$

and $\sigma_{i,j}$ are the natural frequencies. Projections of $\varphi_{i,j}$ on the mean free surface $z = 0$ introduce the shapes of standing waves $f_{i,j}(x, y) = \varphi_{i,j}|_{z=0}$.

Physically, $f_{i,j}$ may be classified in terms of subclasses. The first one consists of two-dimensional Stokes wave shapes in the Oxz- and Oyz-planes. Corresponding natural modes have often been called 'planar' waves (Miles 1994, also used 'rolls' as the name). These are

$$f_i^{(1)}(x) = \cos(\pi i(x + 1/2)), \quad i \geqslant 0, \quad f_j^{(2)}(y) = \cos(\pi j r(y + 1/(2r))), \quad j \geqslant 0. \tag{2.5}$$

Another subclass defines three-dimensional wave patterns (figure 3*a*)

$$f_i^{(1)}(x) f_j^{(2)}(y), \quad i, j \geqslant 1. \tag{2.6}$$

Later analysis will show that it is convenient to introduce the mixed modes also

$$S_1^i(x, y) = f_i^{(1)}(x) - f_i^{(2)}(y), \quad S_2^i(x, y) = f_i^{(1)}(x) + f_i^{(2)}(y), \tag{2.7}$$

recombining two Stokes modes of (2.5) into three-dimensional patterns (see figure 3*b*, *c*). In order to simplify the narrative we will denote them 'diagonal' or (due to Miles 1994) 'square'. If different non-zero weight coefficients are associated with $f_i^{(1)}$ and $f_i^{(2)}$, i.e. $Af_i^{(1)} + Bf_i^{(2)}$, $AB \neq 0$, $|A| \neq |B|$, we call them 'square'-like modes.

The set $\{f_{i,j}(x, y),\ i + j \geqslant 1\}$ represents an appropriate Fourier basis in the horizontal rectangular cross-section of the tank $[-1/2, 1/2] \times [-1/(2r), 1/(2r)]$, and $\{\varphi_{i,j}(x, y, z),\ i + j \geqslant 1\}$ is a complete system of harmonic functions in the unperturbed fluid domain $Q_0 = [-1/2, 1/2] \times [-1/(2r), 1/(2r)] \times [-h, 0]$, which satisfies zero Neumann boundary conditions on the tank surface. Following the general modal

https://doi.org/10.1017/S0022112003004816 Published online by Cambridge University Press

scheme by Faltinsen *et al.* (2000) (see their equations (3.4), (3.6) and (3.7)) we impose solution of (2.1) as

$$\xi(x, y, z, t) = z - f(x, y, t), \quad f(x, y, t) = \beta^{i,j}(t) f_i^{(1)}(x) f_j^{(2)}(y), \tag{2.8}$$

$$\Phi(x, y, z, t) = \boldsymbol{v}_0 \cdot \boldsymbol{P} + \boldsymbol{\omega} \cdot \boldsymbol{\Omega} + R^{i,j}(t)\varphi_{i,j}(x, y, z), \tag{2.9}$$

where the summation is performed by the *repeated upper–lower indexes* $i, j \geqslant 0$, $i + j \neq 0$. Here $\beta^{i,j}(t)$ and $R^{i,j}(t)$ are unknown time-dependent functions governing the evolution of the free surface and the velocity potential. Further, $\boldsymbol{\Omega}(x, y, z, t) = (\Omega_1, \Omega_2, \Omega_3)$ is the Stokes–Zhukovsky potential defined by the Neumann boundary value problem:

$$\left.\begin{aligned} &\Delta\boldsymbol{\Omega} = 0 \quad \text{in} \quad Q(t), \quad \left.\frac{\partial \Omega_1}{\partial \nu}\right|_{S(t)+\Sigma(t)} = y\nu_z - z\nu_y, \\ &\left.\frac{\partial \Omega_2}{\partial \nu}\right|_{S(t)+\Sigma(t)} = z\nu_x - x\nu_z, \quad \left.\frac{\partial \Omega_3}{\partial \nu}\right|_{S(t)+\Sigma(t)} = x\nu_y - y\nu_x, \end{aligned}\right\} \tag{2.10}$$

where ν_x, ν_y, ν_z are the projections of the outer normal onto the $Oxyz$-axes.

We assume that the tank does not perform yaw/heave motions, i.e. $v_{O3} = \omega_3 = 0$ (figure 2). In addition, $\omega_1, \omega_2, v_{O1}, v_{O2}$ and their derivatives define a combined oscillatory sway/surge/roll/pitch forcing which are sufficiently small and of order $\epsilon \ll 1$. Using the general infinite-dimensional modal system of Faltinsen *et al.* (2000) gives the following system of ordinary differential equations coupling $\beta_{i,j}$ and $R_{i,j}$ (a dot over a symbol means the time derivative) derived correct to $O(\epsilon)$ in the forcing terms:

$$\frac{\partial A_{n,k}}{\partial \beta_{i,j}} \dot{\beta}^{i,j} = A_{(n,k)(i,j)} R^{n,k}, \quad n, k = 0, 1, \ldots, \quad n + k \neq 0, \tag{2.11}$$

$$\begin{aligned} &\frac{\partial A_{n,k}}{\partial \beta_{i,j}} \dot{R}^{n,k} + \frac{1}{2} \frac{\partial A_{(n,k),(l,m)}}{\partial \beta_{i,j}} R^{n,k} R^{l,m} + \dot{\omega}_1 \frac{\partial l_{1\omega}}{\partial \beta_{i,j}} + \dot{\omega}_2 \frac{\partial l_{2\omega}}{\partial \beta_{i,j}} + \omega_1 \frac{\partial l_{1\omega t}}{\partial \beta_{i,j}} + \omega_2 \frac{\partial l_{2\omega t}}{\partial \beta_{i,j}} \\ &\quad - \frac{\mathrm{d}}{\mathrm{d}t}\left(\omega_1 \frac{\partial l_{1\omega t}}{\partial \dot{\beta}_{i,j}} + \omega_2 \frac{\partial l_{2\omega t}}{\partial \dot{\beta}_{i,j}}\right) + (\dot{v}_{01} - g_1)\frac{\partial l_1}{\partial \beta_{i,j}} + (\dot{v}_{02} - g_2)\frac{\partial l_2}{\partial \beta_{i,j}} \\ &\quad + (-g_3)\frac{\partial l_3}{\partial \beta_{i,j}} = 0, \quad i, j = 0, 1, \ldots, \quad i + j \neq 0. \end{aligned} \tag{2.12}$$

Here

$$\left.\begin{aligned} &l_{k\omega} = \int_{Q(t)} \Omega_k \,\mathrm{d}Q, \quad l_{k\omega t} = \int_{Q(t)} \frac{\partial \Omega_k}{\partial t} \,\mathrm{d}Q, \\ &l_1 = \int_{Q(t)} x \,\mathrm{d}Q, \quad l_2 = \int_{Q(t)} y \,\mathrm{d}Q, \quad l_3 = \int_{Q(t)} z \,\mathrm{d}Q, \\ &A_{n,k} = \int_{Q(t)} \varphi_{n,k} \,\mathrm{d}Q, \quad A_{(n,k),(i,j)} = \int_{Q(t)} (\nabla\varphi_{n,k}, \nabla\varphi_{i,j}) \,\mathrm{d}Q \end{aligned}\right\} \tag{2.13}$$

are nonlinear functions of $\beta_{l,m}$.

Although we neglect forcing terms which are of $o(\epsilon)$, this system does not account for the smallness of the generalized coordinates $\beta_{i,j}$ and $R_{n,k}$. This must be done after ordering them relative to the forcing amplitude.

https://doi.org/10.1017/S0022112003004816 Published online by Cambridge University Press

2.3. *Third-order adaptive modal system*

Analytical studies devoted to two-dimensional sloshing as well as existing asymptotic schemes for three-dimensional nonlinear sloshing with finite fluid depth are almost always based on third-order relationships between the fluid amplitude response and the forcing. This implies an infinite number of $\beta_{i,j}$ and $R_{i,j}$, restricted by $\beta_{i,j} \lesssim O(\epsilon^{1/3})$, $R_{i,j} \lesssim O(\epsilon^{1/3})$. Examples are the adaptive modal system by Faltinsen & Timokha (2001) and the third-order equation by Zakharov (1968). These assume an equal contribution from all the modes, i.e.

$$\beta_{i,j} \sim R_{i,j} = O(\epsilon^{1/3}), \quad i+j \geqslant 1, \tag{2.14}$$

related to the forcing amplitude ϵ.

Accounting for (2.14) in (2.11)–(2.13) and keeping the terms of $O(\epsilon)$ gives the following infinite-dimensional modal system coupling $\beta_{i,j}$:

$$\begin{aligned}
&\ddot{\beta}^{a,b}\left[\delta_{ia}\delta_{jb} + d^{1,(i,j)}_{(a,b),(c,d)}\beta^{c,d} + d^{2,(i,j)}_{(a,b),(c,d),(e,f)}\beta^{c,d}\beta^{e,f}\right] + \sigma^2_{i,j}\beta_{i,j} \\
&\quad + \dot{\beta}^{a,b}\dot{\beta}^{c,d}\left[t^{0,(i,j)}_{(a,b),(c,d)} + t^{1,(i,j)}_{(a,b),(c,d),(e,f)}\beta^{e,f}\right] + P^{(2)}_{i,j}\left[\dot{v}_{O2} + S^{(2)}_j\ddot{\psi}_1 + g\psi_1\right] \\
&\quad + P^{(1)}_{i,j}\left[\dot{v}_{O1} - S^{(1)}_i\ddot{\psi}_2 - g\psi_2\right] = 0, \quad i+j \geqslant 1,
\end{aligned} \tag{2.15}$$

where all the coefficients (tensors $\boldsymbol{d}, \boldsymbol{t}, \boldsymbol{P}$ and $\boldsymbol{S}$) are calculated explicitly in Appendix A as functions of h. The derivation of (2.15) became particularly tedious and analytically difficult compared to analogous analytical manipulations for two-dimensional sloshing by Faltinsen & Timokha (2001). Hydrodynamic forces and moments can be found in terms of $\beta_{i,j}$. This is not further pursued in this paper.

The system (2.15) captures progressive nonlinear activation of an infinite set of natural modes in the framework of a third-order theory. An appropriate mechanism of amplification may be the secondary (internal) resonance (see Bridges 1985, 1987; Bryant 1989; Ockendon *et al.* 1996; Faltinsen & Timokha 2002*a*). The system (2.15) needs the initial conditions

$$\beta_{i,j} = \alpha^0_{i,j}, \quad \dot{\beta}_{i,j} = \alpha^1_{i,j}, \quad i+j \geqslant 1, \tag{2.16}$$

where the known constants $\alpha^0_{i,j}$ and $\alpha^1_{i,j}$ describe the initial fluid shape and the initial velocity respectively. These constants may be obtained from Fourier treatment of (2.2). For periodic forcing we can also employ the periodic conditions (equivalent to (2.3))

$$\beta_{i,j}(t+T) = \beta_{i,j}(t), \quad \dot{\beta}_{i,j}(t+T) = \dot{\beta}_{i,j}(t), \quad i+j \geqslant 1, \tag{2.17}$$

where T is the forcing period.

The system (2.15) together with (2.16) (or (2.17) may be truncated and implemented for numerical analysis of the fluid sloshing as in Perko-like methods (see, for instance, recent papers by La Rocca *et al.* 1997; La Rocca, Sciortino & Boniforti 2000; Shankar & Kidambi 2002). For periodic forcing the numerical approach makes it also possible to treat the periodic steady-state solutions including bifurcation and stability analysis by employing appropriate codes given by Bader & Ascher (1987) and Hermann & Ullrich (1992). Another way (Faltinsen & Timokha 2001) consists in preliminary asymptotic simplification of (2.15) with the selection of leading modes and then reduction to a nonlinear finite-dimension system. This may lead to a modal system of less accuracy but provides much more time-efficient and robust simulations.

https://doi.org/10.1017/S0022112003004816 Published online by Cambridge University Press

3. Sloshing in a square-base basin

3.1. *Asymptotic modal system for near-square cross-section*

Moving to square geometry implies $\sigma_{i,j} \to \sigma_{j,i}$ $(r \to 1)$ and, therefore, the pair of primary natural modes $f_1^{(1)}$ and $f_1^{(2)}$ becomes degenerate (having equal natural frequencies). Analysing the secondary (internal) resonance relationships for higher modes $\sigma_{i,j} \approx 2\sigma_{1,0}, i+j=2$; $\sigma_{i,j} \approx 3\sigma_{1,0}, i+j=3$ etc. for $r=1$ we find these are not satisfied for finite (non-shallow) h. Amplification of the modal functions $\beta_{i,j}$ will basically depend on external forcing and initial conditions. Fundamental experimental studies by Abramson (1966) and Mikishev (1978) showed that maximum wave amplification due to surge/sway/pitch/roll excitation occurs when external forcing is periodic and close to the lowest natural frequency (here $\sigma_{1,0} \approx \sigma_{0,1}$). The asymptotic limit $\epsilon \to 0$ then suggests only two primary leading modes. Accounting for the structure of (2.15) yields

$$\left.\begin{aligned} &\beta_{1,0} \sim \beta_{0,1} = O\left(\epsilon^{1/3}\right), \quad \beta_{2,0} \sim \beta_{1,1} \sim \beta_{0,2} = O\left(\epsilon^{2/3}\right), \\ &\beta_{3,0} \sim \beta_{2,1} \sim \beta_{1,2} \sim \beta_{0,3} = O(\epsilon), \quad \beta_{i,j} \lesssim O(\epsilon),\ i+j \geqslant 4 \end{aligned}\right\} \tag{3.1}$$

in terms of ϵ.

These relationships are consistent with the Moiseyev third-order assumptions in the form given by Faltinsen *et al.* (2000) leading to the single dominant modal theory for two-dimensional sloshing. The calculation shows that (3.1) reduces (2.15) to a finite-dimensional system of nonlinear ordinary differential equations coupling $\beta_{i,j}$, $i+j \leqslant 3$. Other modes $(i+j \geqslant 4)$ are easily governed by the linear sloshing theory. After re-denoting for brevity

$$\left.\begin{aligned} &\beta_{1,0} = a_1, \quad \beta_{2,0} = a_2, \quad \beta_{0,1} = b_1, \quad \beta_{0,2} = b_2, \quad \beta_{1,1} = c_1, \\ &\beta_{3,0} = a_3, \quad \beta_{2,1} = c_{21}, \quad \beta_{1,2} = c_{12}, \quad \beta_{0,3} = b_3 \end{aligned}\right\} \tag{3.2}$$

the modal system for (2.15) can be re-written in the following approximate form:

$$\begin{aligned} &\left[\ddot{a}_1 + \sigma_{1,0}^2 a_1 + d_1(\ddot{a}_1 a_2 + \dot{a}_1 \dot{a}_2) + d_2\left(\ddot{a}_1 a_1^2 + \dot{a}_1^2 a_1\right) + d_3 \ddot{a}_2 a_1 \right. \\ &\quad \left. + P_{1,0}^{(1)}\left(\dot{v}_{O1} - S_1^{(1)} \ddot{\psi}_2 - g\psi_2\right)\right] + d_6 \ddot{a}_1 b_1^2 + \ddot{b}_1(d_7 c_1 + d_8 a_1 b_1) + d_9 \ddot{c}_1 b_1 \\ &\quad + d_{10} \dot{b}_1^2 a_1 + d_{11} \dot{a}_1 \dot{b}_1 b_1 + d_{12} \dot{b}_1 \dot{c}_1 = 0, \end{aligned} \tag{3.3a}$$

$$\begin{aligned} &\left[\ddot{b}_1 + \sigma_{0,1}^2 b_1 + \bar{d}_1(\ddot{b}_1 b_2 + \dot{b}_1 \dot{b}_2) + \bar{d}_2\left(\ddot{b}_1 b_1^2 + \dot{b}_1^2 b_1\right) + \bar{d}_3 \ddot{b}_2 b_1 \right. \\ &\quad \left. + P_{0,1}^{(2)}\left(\dot{v}_{O2} + S_1^{(2)} \ddot{\psi}_1 + g\psi_1\right)\right] + \bar{d}_6 \ddot{b}_1 a_1^2 + \ddot{a}_1(\bar{d}_7 c_1 + \bar{d}_8 a_1 b_1) + \bar{d}_9 \ddot{c}_1 a_1 \\ &\quad + \bar{d}_{10} \dot{a}_1^2 b_1 + \bar{d}_{11} \dot{a}_1 \dot{b}_1 a_1 + \bar{d}_{12} \dot{a}_1 \dot{c}_1 = 0, \end{aligned} \tag{3.3b}$$

$$\left[\ddot{a}_2 + \sigma_{2,0}^2 a_2 + d_4 \ddot{a}_1 a_1 + d_5 \dot{a}_1^2\right] = 0, \tag{3.3c}$$

$$\left[\ddot{b}_2 + \sigma_{0,2}^2 b_2 + \bar{d}_4 \ddot{b}_1 b_1 + \bar{d}_5 \dot{b}_1^2\right] = 0, \tag{3.3d}$$

$$\ddot{c}_1 + \hat{d}_1 \ddot{a}_1 b_1 + \hat{d}_2 \ddot{b}_1 a_1 + \hat{d}_3 \dot{a}_1 \dot{b}_1 + \sigma_{1,1}^2 c_1 = 0, \tag{3.3e}$$

$$\begin{aligned} &\left[\ddot{a}_3 + \sigma_{3,0}^2 a_3 + \ddot{a}_1\left(q_1 a_2 + q_2 a_1^2\right) + q_3 \ddot{a}_2 a_1 + q_4 \dot{a}_1^2 a_1 + q_5 \dot{a}_1 \dot{a}_2 \right. \\ &\qquad \left. + P_{3,0}^{(1)}[\dot{v}_{O1} - S_3^{(1)} \ddot{\psi}_2 - g\psi_2]\right] = 0, \end{aligned} \tag{3.4a}$$

$$\begin{aligned} &\ddot{c}_{21} + \sigma_{2,1}^2 c_{21} + \ddot{a}_1(q_6 c_1 + q_7 a_1 b_1) + \ddot{b}_1\left(q_8 a_2 + q_9 a_1^2\right) + q_{10} \ddot{a}_2 b_1 + q_{11} \ddot{c}_1 a_1 \\ &\qquad + q_{12} \dot{a}_1^2 b_1 + q_{13} \dot{a}_1 \dot{b}_1 a_1 + q_{14} \dot{a}_1 \dot{c}_1 + q_{15} \dot{a}_2 \dot{b}_1 = 0, \end{aligned} \tag{3.4b}$$

https://doi.org/10.1017/S0022112003004816 Published online by Cambridge University Press

$$\ddot{c}_{12}+\sigma_{1,2}^2 c_{12}+\ddot{b}_1(\bar{q}_6 c_1+\bar{q}_7 a_1 b_1)+\ddot{a}_1(\bar{q}_8 b_2+\bar{q}_9 b_1^2)+\bar{q}_{10}\ddot{b}_2 a_1+\bar{q}_{11}\ddot{c}_1 b_1 + \bar{q}_{12}\dot{b}_1^2 a_1+\bar{q}_{13}\dot{a}_1\dot{b}_1 b_1\bar{q}_{14}\dot{b}_1\dot{c}_1+\bar{q}_{15}\dot{a}_1\dot{b}_2=0, \quad (3.4c)$$

$$\left[\ddot{b}_3+\sigma_{0,3}^2 b_3+\ddot{b}_1\left(\bar{q}_1 b_2+\bar{q}_2 b_1^2\right)+\bar{q}_3\ddot{b}_2 b_1+\bar{q}_4\dot{b}_1^2 b_1+\bar{q}_5\dot{b}_1\dot{b}_2 + P_{0,3}^{(2)}\left[\dot{v}_{O2}+S_3^{(2)}\ddot{\psi}_1+g\psi_1\right]\right]=0 \quad (3.4d)$$

with coefficients $d_i(h), \bar{d}_i(h), \hat{d}_i(h), q_i(h)$ and $\bar{q}_i(h)$ calculated by formulae in Appendix B. The higher modes are governed by linear equations:

$$\ddot{\beta}_{i,j}+\sigma_{i,j}\beta_{i,j}+P_{i,j}^{(2)}\left[\dot{v}_{O2}+S_j^{(2)}\ddot{\psi}_1+g\psi_i\right]+P_{i,j}^{(1)}\left[\dot{v}_{O1}-S_i^{(1)}\ddot{\psi}_2-g\psi_2\right]=0, \quad i+j\geqslant 4. \quad (3.5)$$

We see in (3.3), (3.4) that the terms in square brackets are associated with 'planar' flows in either Oxz- or Oyz-planes. They are exactly the same as derived by Faltinsen *et al.* (2000). Other terms and additional equations for c_{11}, c_{21} and c_{12} are due to three-dimensional intermodal interaction. Here the subsystem (3.3) is complete in a_1, b_1, a_2, b_2 and c_1 and does not depend on a_3, c_{21}, c_{12} and b_3 calculated from (3.4). The subsystem (3.4) is linear in a_3, c_{21}, c_{12} and b_3 and depends nonlinearly on a_1, b_1, a_2, b_2 and c_1.

The asymptotic system (3.3)–(3.5) is the main mathematical object of this paper. It is formally of infinite degrees of freedoms and, therefore, needs the initial (2.16) or periodical (2.17) conditions for all the modes. However, only nine degrees of freedom (equations (3.3) and (3.4)) are nonlinearly coupled. When we know the forcing terms and initial (or periodic) conditions explicitly, we can easily integrate the system's linear (infinite) subsystem (3.5). The actual analysis reduces to the nonlinear part (3.3), (3.4).

3.2. *Steady-state motions due to resonant harmonic excitation*

Let us assume that the external forcing is a harmonic function of time. Although this can imply phase shifts in $\dot{v}_{Oi}$ and ψ_i $(\omega_i=\dot{\psi}_i)$, $i=1,2$, we concentrate without loss of generality on the synchronized horizontal/angular harmonic excitation, i.e. $\dot{v}_{Oi}=-\sigma^2 H_i\cos\sigma t$, $\psi_i=\psi_{0i}\cos\sigma t$ and $\omega_i=-\sigma\psi_{0i}\sin\sigma t$, $i=1,2$ with

$$H_1=H\cos\theta_1, \quad H_2=\sin\theta_2; \quad \psi_1=\psi_0\cos\theta_2, \quad \psi_2=\psi_0\sin\theta_2 \quad (3.6)$$

(H is the amplitude of translatory excitation, ψ_0 is the angular amplitude and $(\cos\theta_i,\sin\theta_i)$, $i=1,2$, are the guiding vectors for these excitations). This transforms the forcing terms in (3.3*a*), (3.3*b*), (3.4*a*) and (3.4*d*) to the following form:

$$\left.\begin{aligned}
-\sigma^2 P_1\cos\sigma t&=\left[\sigma^2 P_{1,0}^{(1)}\left(-H_1+\psi_{02}\left(S_1^{(1)}-g/\sigma^2\right)\right)\right]\cos\sigma t,\\
-\sigma^2 P_2\cos\sigma t&=\left[\sigma^2 P_{0,1}^{(2)}\left(-H_2+\psi_{01}\left(-S_1^{(2)}+g/\sigma^2\right)\right)\right]\cos\sigma t,\\
-\sigma^2 P_3\cos\sigma t&=\left[\sigma^2 P_{3,0}^{(1)}\left(-H_1+\psi_{02}\left(S_3^{(1)}-g/\sigma^2\right)\right)\right]\cos\sigma t,\\
-\sigma^2 P_4\cos\sigma t&=\left[\sigma^2 P_{0,3}^{(2)}\left(-H_2+\psi_{01}\left(-S_3^{(1)}+g/\sigma^2\right)\right)\right]\cos\sigma t.
\end{aligned}\right\} \quad (3.7)$$

The modal system with (3.7) can be asymptotically integrated for steady-state solutions by the combining the Bubnov–Galerkin method with asymptotic expansions.

https://doi.org/10.1017/S0022112003004816 Published online by Cambridge University Press

The procedure was described in some detail by Faltinsen *et al.* (2000). The result is

$$\left.\begin{aligned} a_1 &= A\cos\sigma t + \bar{A}\sin\sigma t + \{[A(n_1(-A^2+3\bar{A}) + n_2(B^2-\bar{B}^2)) + 2n_2B\bar{A}\bar{B}]\cos 3\sigma t \\ &\quad + [\bar{A}(n_1(\bar{A}^2-3A^2) + n_2(B^2-\bar{B}^2)) - 2n_2AB\bar{B}]\sin 3\sigma t\}/\left(9-\bar{\sigma}_{1,0}^2\right) + o(\epsilon), \\ b_1 &= \bar{B}\cos\sigma t + B\sin\sigma t + \{[\bar{B}(\bar{n}_1(-\bar{B}^2+3B^2) + \bar{n}_2(\bar{A}^2-A^2)) + 2\bar{n}_2AB\bar{A}]\cos 3\sigma t \\ &\quad + [B(\bar{n}_1(B^2-3\bar{B}^2) + \bar{n}_2(\bar{A}^2-A^2)) - 2\bar{n}_2A\bar{A}\bar{B}]\sin 3\sigma t\}/\left(9-\bar{\sigma}_{0,1}^2\right) + o(\epsilon), \end{aligned}\right\} \tag{3.8a}$$

$$\left.\begin{aligned} a_2 &= p_0(A^2+\bar{A}^2) + h_0(A^2-\bar{A}^2)\cos 2\sigma t + 2h_0A\bar{A}\sin 2\sigma t + o(\epsilon), \\ b_2 &= \bar{p}_0(\bar{B}^2+B^2) + \bar{h}_0(\bar{B}^2-B^2)\cos 2\sigma t + 2\bar{h}_0\bar{B}B\sin 2\sigma t + o(\epsilon), \\ c_1 &= p_1(A\bar{B}+\bar{A}B) + h_1(A\bar{B}-\bar{A}B)\cos 2\sigma t + h_1(\bar{A}\bar{B}+AB)\sin 2\sigma t + o(\epsilon), \end{aligned}\right\} \tag{3.8b}$$

$$\left.\begin{aligned} a_3 &= \{N_1[(A^3+A\bar{A}^2)\cos\sigma t + (A^2\bar{A}+\bar{A}^3)\sin\sigma t] + P_3\cos\sigma t\}/(1-\bar{\sigma}_{3,0}) \\ &\quad + N_2\{(-A^3+3A\bar{A}^2)\cos 3\sigma t + (\bar{A}^3-3A^2\bar{A})\sin 3\sigma t\}/\left(9-\bar{\sigma}_{3,0}^2\right) + o(\epsilon), \\ c_{21} &= \{(N_3\bar{A}^2\bar{B} + (N_4-N_3)AB\bar{A} + N_4A^2\bar{B})\cos\sigma t + (N_3A^2B \\ &\quad + (N_4-N_3)A\bar{B}\bar{A} + N_4\bar{A}^2B)\sin\sigma t\}/(1-\bar{\sigma}_{2,1}) + N_5\{(\bar{A}^2\bar{B} + 2AB\bar{A} \\ &\quad - A^2\bar{B})\cos 3\sigma t + (B\bar{A}^2 - 2A\bar{A}\bar{B} - A^2B)\sin 3\sigma t\}/(9-\bar{\sigma}_{2,1}) + o(\epsilon), \\ c_{12} &= \{(\bar{N}_3AB^2 + (\bar{N}_4-\bar{N}_3)B\bar{A}\bar{B} + \bar{N}_4A\bar{B}^2)\cos\sigma t + (\bar{N}_3\bar{B}^2\bar{A} \\ &\quad + (\bar{N}_4-\bar{N}_3)B\bar{B} + \bar{N}_4B^2\bar{A}^2)\sin\sigma t\}/\left(1-\bar{\sigma}_{1,2}^2\right) + \bar{N}_5\{(AB^2 + 2\bar{A}B\bar{B} \\ &\quad - A\bar{B}^2)\cos 3\sigma t + (\bar{A}B^2 - 2AB\bar{B} - \bar{A}\bar{B}^2)\sin 3\sigma t\}/\left(9-\bar{\sigma}_{1,2}^2\right) + o(\epsilon), \\ b_3 &= \{\bar{N}_1[(\bar{B}^3+\bar{B}B^2)\cos\sigma t + (B\bar{B}^2+B^3)\sin\sigma t] + P_4\cos\sigma t\}/\left(1-\bar{\sigma}_{0,3}^2\right) \\ &\quad + \bar{N}_2\{(-\bar{B}^3+3B^2\bar{B})\cos 3\sigma t + (B^3-3B\bar{B}^2)\sin 3\sigma t\}/\left(9-\bar{\sigma}_{0,3}^2\right) + o(\epsilon) \end{aligned}\right\} \tag{3.8c}$$

with

$$p_0 = \frac{d_4-d_5}{2\bar{\sigma}_{2,0}^2}, \quad \bar{p}_0 = \frac{\bar{d}_4-\bar{d}_5}{2\bar{\sigma}_{0,2}^2}, \quad h_0 = \frac{d_4+d_5}{2\left(\bar{\sigma}_{2,0}^2-4\right)}, \quad \bar{h}_0 = \frac{\bar{d}_4+\bar{d}_5}{2\left(\bar{\sigma}_{0,2}^2-4\right)},$$
$$p_1 = \frac{\hat{d}_1+\hat{d}_2-\hat{d}_3}{2\bar{\sigma}_{1,1}^2}, \quad h_1 = \frac{\hat{d}_1+\hat{d}_2+\hat{d}_3}{2\left(\bar{\sigma}_{1,1}^2-4\right)},$$

and

$$\begin{aligned} n_1 &= \tfrac{1}{2}d_2 + h_0\left(\tfrac{3}{2}d_1 + 2d_3\right), \\ n_2 &= \tfrac{1}{4}(d_6+d_8+d_{10}+d_{11}) + h_1\left(\tfrac{1}{2}d_7 + 2d_9 + d_{12}\right), \\ N_1 &= -\tfrac{3}{4}q_2 + \tfrac{1}{4}q_4 + h_0\left(-\tfrac{1}{2}q_1 - 2q_3 + q_5\right) - q_1p_0, \\ N_2 &= \tfrac{1}{4}q_2 + \tfrac{1}{4}q_4 + h_0\left(\tfrac{1}{2}q_1 + 2q_3 + q_5\right), \\ N_3 &= -\tfrac{1}{4}q_7 - \tfrac{1}{4}q_9 + \tfrac{3}{4}q_{12} - \tfrac{1}{4}q_{13} + h_0\left(\tfrac{1}{2}q_8 + 2q_{10} - q_{15}\right) - q_8p_0 + h_1\left(-\tfrac{1}{2}q_6 - 2q_{11} + q_{14}\right), \\ N_4 &= -\tfrac{3}{4}q_7 - \tfrac{3}{4}q_9 + \tfrac{1}{4}q_{12} + \tfrac{1}{4}q_{13} + h_0\left(-\tfrac{1}{2}q_8 - 2q_{10} + q_{15}\right) - q_8p_0 \\ &\quad + h_1\left(-\tfrac{1}{2}q_6 - 2q_{11} + q_{14}\right) - q_6p_1, \\ N_5 &= \tfrac{1}{4}q_7 + \tfrac{1}{4}q_9 + \tfrac{1}{4}q_{12} + \tfrac{1}{4}q_{13} + h_0\left(\tfrac{1}{2}q_8 + 2q_{10} + q_{15}\right) + h_1\left(\tfrac{1}{2}q_6 + 2q_{11} + q_{14}\right), \end{aligned}$$

where

$$\bar{\sigma}_{i,j}^2 = \frac{\sigma_{i,j}^2}{\sigma^2} \tag{3.9}$$

https://doi.org/10.1017/S0022112003004816 Published online by Cambridge University Press

and $\bar{n}_i$, $\bar{N}_i$ can be obtained by adding bars over d_i, p_i and h_i in the expressions for n_i and N_i.

The terms in the expressions for a_1 and b_1 are of a different order. The primary amplitudes $A, \bar{A}, \bar{B}$ and B are associated with $O(\epsilon^{1/3})$ while the expressions in the following lines are $O(\epsilon)$. The primary amplitudes can be found by inserting (3.8*a*) into (3.3*a*) and (3.3*b*) and collecting the terms proportional to $\cos\sigma t$ and $\sin\sigma t$. This gives the following secular system of algebraic equations:

$$\left.\begin{aligned}
&A\left((\bar{\sigma}_{1,0}^2-1)+m_1(A^2+\bar{A}^2)+m_2\bar{B}^2+m_3B^2\right)+(m_2-m_3)\bar{A}\bar{B}B-P_1=0,\\
&\bar{A}\left((\bar{\sigma}_{1,0}^2-1)+m_1(A^2+\bar{A}^2)+m_2B^2+m_3\bar{B}^2\right)+(m_2-m_3)AB\bar{B}=0,\\
&\bar{B}\left((\bar{\sigma}_{0,1}^2-1)+\bar{m}_1(B^2+\bar{B}^2)+\bar{m}_2A^2+\bar{m}_3\bar{A}^2\right)+(\bar{m}_2-\bar{m}_3)\bar{A}AB-P_2=0,\\
&B\left((\bar{\sigma}_{0,1}^2-1)+\bar{m}_1(B^2+\bar{B}^2)+\bar{m}_2\bar{A}^2+\bar{m}_3A^2\right)+(\bar{m}_2-\bar{m}_3)\bar{A}A\bar{B}=0,
\end{aligned}\right\} \tag{3.10}$$

where

$$\left.\begin{aligned}
m_1&=-\tfrac{1}{2}d_2-d_1\left(p_0-\tfrac{1}{2}h_0\right)-2h_0d_3,\\
m_2&=-\tfrac{3}{4}d_6+\tfrac{1}{4}d_{10}-\tfrac{3}{4}d_8+\tfrac{1}{4}d_{11}-d_7p_1-h_1\left(\tfrac{1}{2}d_7+2d_9-d_{12}\right),\\
m_3&=-\tfrac{1}{4}d_6+\tfrac{3}{4}d_{10}-\tfrac{1}{4}d_8-\tfrac{1}{4}d_{11}-h_1\left(\tfrac{1}{2}d_7+2d_9-d_{12}\right)
\end{aligned}\right\} \tag{3.11}$$

and $\bar{m}_i, i=1,2,3$ are obtained from (3.11) by adding bars over d_i, p_i and h_i. The system of nonlinear algebraic equations (3.10) generalizes the single secular equation obtained by Faltinsen *et al.* (2000) (see their equation (6.8) containing only m_1) to the three-dimensional case. It does not always have solutions and may have multiple solutions. This depends on the values of m_i and $\bar{m}_i$. Faltinsen & Timokha (2001) emphasized also that contrary to standard Moiseyev-type analysis the secular equations derived from the modal theories include coefficients which vary not only with h (r for a rectangular cross-section), but also with σ. This is caused by our Bubnov-Galerkin technique which does not require the Moiseyev detuning $\bar{\sigma}_{1,0}^2-1=O(\epsilon^{2/3})$. This situation was extensively discussed by Faltinsen & Timokha (2001) in the context of applicability of the asymptotic methods when σ drifts slightly away of the primary resonance. This discussion was related to two-dimensional sloshing with critical depth h_1 when $m_1\to 0$. While the standard Moiseyev technique establishes in this case a linear response, the secular equations with varying m_1 capture nonlinearities away from a small vicinity of the main resonance. In many cases an improved agreement with experimental data is obtained.

Another important remark is that by assuming slowly varying amplitudes $A, \bar{A}, B$ and B we can derive from our modal system a dynamic system, where the left-hand sides of (3.10) become its right-hand sides (in normal form). This system is equivalent to the Hamiltonian systems already derived by Feng & Sethna (1989) and Bridges (1986), but with other forcing terms and the coefficients depending on the excitation frequency (the Moiseyev detuning). However, focusing exclusively on this system neglects contributions of higher modes and their strong dependence on initial conditions. Another important point is that some terms of $O(\epsilon)$ give, in real calculations, significant contributions to sloshing relative to formal dominant terms. This point was exemplified by Faltinsen (1974), La Rocca *et al.* (1997) and Faltinsen *et al.* (2000). Gavrilyuk, Lukovsky & Timokha (2000) also showed an effect of these terms on the mobility of the nodal line.

https://doi.org/10.1017/S0022112003004816 Published online by Cambridge University Press

The following analysis assumes $r = 1$, i.e. a square-base tank. This means

$$\bar{\sigma}_1 \overset{def}{=} \bar{\sigma}_{1,0} = \bar{\sigma}_{0,1}, \quad \bar{\sigma}_{i,j} = \bar{\sigma}_{j,i}, \quad \bar{d}_i = d_i, \quad m_1 = \bar{m}_1, \quad m_2 = \bar{m}_2, \quad m_3 = \bar{m}_3, \tag{3.12}$$

where m_i are functions of h and σ. Resonant bifurcations due to perturbed r as investigated by Bridges (1985) will not be studied.

3.3. *Stability of the steady-state motions*

After calculation of periodic solutions $a_1, b_1, \ldots, b_3$ we can apply any one of numerous methods to study their stability. One way is to implement the Floquet–Lyapunov scheme (Lukovsky 1990), which assumes perturbations of all the modes. However, we assume that only perturbations in a_1 and b_1 are important, introduce the slowly varying time $\tau = \epsilon^{2/3}\sigma t/2$, the Moiseyev asymptotics $\bar{\sigma}_1^2 - 1 = O(\epsilon^{2/3})$ and express the infinitesimally perturbed dominant solutions as

$$\left.\begin{aligned} a_1 &= (A + \alpha(\tau))\cos\sigma t + (\bar{A} + \bar{\alpha}(\tau))\sin\sigma t + o(\epsilon^{1/3}), \\ b_1 &= (\bar{B} + \bar{\beta}(\tau))\cos\sigma t + (B + \beta(\tau))\sin\sigma t + o(\epsilon^{1/3}), \end{aligned}\right\} \tag{3.13}$$

where A, $\bar{A}$, B and $\bar{B}$ are the solutions of (3.10) and $\alpha, \bar{\alpha}, \beta$ and $\bar{\beta}$ are their relative perturbations depending on τ. A similar procedure is applicable to the Hamiltonian systems governing slow-time evolution of the primary amplitudes. Inserting (3.13) into (3.3)–(3.4), collecting terms of the lowest asymptotic order and keeping linear terms in $\alpha, \bar{\alpha}, \beta$ and $\bar{\beta}$ leads to the following linear system of ordinary differential equations:

$$\boldsymbol{c}' + [\delta\boldsymbol{c}] + \mathscr{C}\boldsymbol{c} = 0, \tag{3.14}$$

where an auxiliary damping term $\delta > 0$ is incorporated in the square brackets. The results below are obtained in the limit $\delta \to 0$. Further, $\boldsymbol{c} = (\alpha, \bar{\alpha}, \beta, \bar{\beta})^T$ and the matrix $\mathscr{C}$ has the following elements:

$$\begin{aligned}
&c_{11} = -[2A\bar{A}m_1 + (m_2 - m_3)B\bar{B}], \ c_{12} = -\left[\bar{\sigma}_1^2 - 1 + m_1A^2 + 3m_1\bar{A}^2 + m_2B^2 + m_3\bar{B}^2\right], \\
&c_{13} = -[2\bar{A}Bm_2 + (m_2 - m_3)A\bar{B}], \ c_{14} = -[2\bar{A}\bar{B}m_3 + (m_2 - m_3)AB], \\
&c_{21} = \bar{\sigma}_1^2 - 1 + 3m_1A^2 + m_1\bar{A}^2 + m_2\bar{B}^2 + m_3B^2, \ c_{22} = 2A\bar{A}m_1 + (m_2 - m_3)B\bar{B}, \\
&c_{23} = 2ABm_3 + (m_2 - m_3)\bar{A}\bar{B}, \ c_{24} = 2A\bar{B}m_2 + (m_2 - m_3)\bar{A}B, \\
&c_{31} = 2m_2A\bar{B} + (m_2 - m_3)B\bar{A}, \ c_{32} = 2m_3\bar{A}\bar{B} + (m_2 - m_3)AB, \\
&c_{33} = 2m_1B\bar{B} + (m_2 - m_3)A\bar{A}, \ c_{34} = \bar{\sigma}_1^2 - 1 + m_1B^2 + 3m_1\bar{B}^2 + m_2A^2 + m_3\bar{A}^2, \\
&c_{41} = -[2m_3AB + (m_2 - m_3)\bar{A}\bar{B}], \ c_{42} = -[2\bar{A}Bm_2 + (m_2 - m_3)A\bar{B}], \\
&c_{43} = -\left[\bar{\sigma}_1^2 - 1 + 3m_1B^2 + m_1\bar{B}^2 + m_2\bar{A}^2 + m_3A^2\right], \ c_{44} = -[2B\bar{B}m_1 + (m_2 - m_3)A\bar{A}].
\end{aligned}$$

The stability of a fixed-point solution can be evaluated by studying (3.14). Its fundamental solution depends on the eigenvalue problem $\det[(\lambda + \delta)E + C] = 0$. Computations (using the analytical manipulator of Waterloo Maple 6) give the following characteristic polynomial:

$$(\lambda + \delta)^4 + c_1(\lambda + \delta)^2 + c_0 = 0, \tag{3.15}$$

where c_0 is the determinant of $\mathscr{C}$ and c_1 is a complicated function of the elements of $\mathscr{C}$. Since the eigenvalues λ can be expressed as $-\delta \pm \sqrt{x_{1,2}}$ ($x_{1,2}$ are solutions of the equation $x^2 + c_1x + c_0 = 0$), the asymptotic stability of the fixed-point solutions

https://doi.org/10.1017/S0022112003004816 Published online by Cambridge University Press

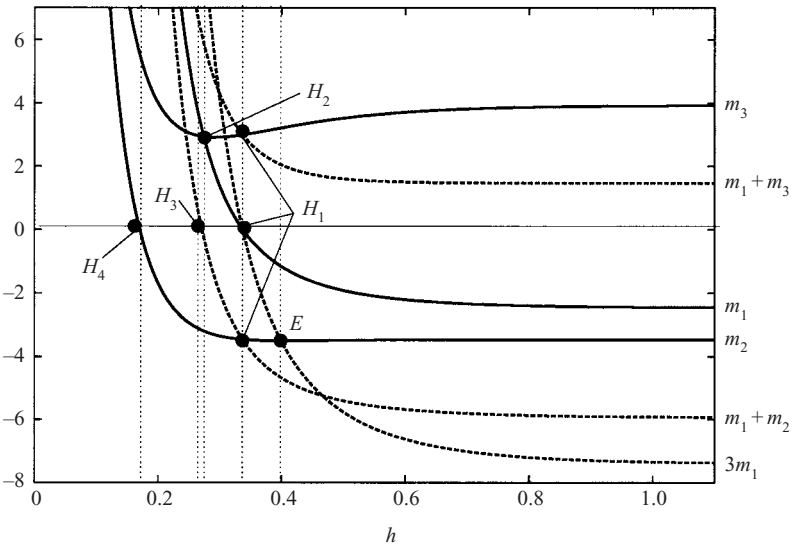


FIGURE 4. Graphs representing $m_i(h, \sigma_1), i = 1, 2, 3$ and some of their linear combinations versus depth/breadth ratio h for a square-base basin. The point H_1 ($m_1 = 0, h_1 = 0.337\ldots$) denotes the 'soft/hard' spring change for the 'planar' steady-state waves (3.20). The point H_2 ($m_1 = m_3$) defines another critical depth $h_2 = 0.274\ldots$, where the solvability condition (3.26) of the secular equations for the 'swirling' mode is not satisfied. The point H_3 denotes the depth $h_3 = 0.27\ldots$ where the 'soft/hard' spring change in the response of a 'square'-like mode (3.21) occurs, and the critical point H_4 denotes the depth $h_4 = 0.17\ldots$, where $m_2 = 0$. In addition, the auxiliary point E corresponds to $h_5 = 0.4\ldots$ obtained from the condition $m_2 = 3m_1$.

means for $\delta \to 0$ that

$$c_0 > 0, \quad c_1 > 0, \quad c_1^2 - 4c_1 > 0. \tag{3.16}$$

Here c_0 vanishes at the turning-point solutions and at the Poincaré bifurcation points. The zeros of the discriminant $c_1^2 - 4c_1$ are Hopf-bifurcation points where the real parts of a pair of complex-conjugate zeros of c_0 become positive.

In general, $P_1 \neq 0$ and $P_2 \neq 0$ for a combined sway/surge and roll/pitch forcing. However, the examination below considers two model situations: $P_1 \neq 0$, $P_2 = 0$ (combined surge/pitch or 'longitudinal' excitation) and $P_1 = P_2 \neq 0$ (diagonal excitation).

3.4. *Steady-state resonant sloshing due to longitudinal excitations* ($r = 1$, $P_1 \neq 0$, $P_2 = 0$)

The amplitudes A, $\bar{A}$, $\bar{B}$ and B of steady-state solutions depend on $m_i = m_i(h, \sigma), i = 1, 2, 3$. Assuming the resonance condition $\sigma \approx \sigma_1$ implies that the steady-state solutions are mainly functions of h. There are critical values of h_i causing (3.10) to have a singular character (insoluble, leading to bifurcation points or hydrodynamically unstable solutions etc.). Some preliminary discussions will be made using figure 4, showing $m_i(h, \sigma_1)$ (and some of their linear combinations) versus h for surge/pitch (longitudinal) excitations. These critical depths are denoted as h_i (points H_i in the graphs). We note that $m_i(h, \sigma_1)$ are approximately constant for $1 \lesssim h$ and vary slowly with h for $1 > h > h_1$. Here $h_1 = 0.337\ldots$ is associated with the change from a soft to hard spring type of 'planar' wave response (depth h_1 came from the analysis of two-dimensional sloshing in a rectangular tank by Fultz 1962; Waterhouse 1994; Faltinsen *et al.* 2000). Lower depths introduce the critical depths $h_2 = 0.274\ldots$ (point $H_2, m_1 = m_3$), $h_3 = 0.27\ldots$ (point $H_3, m_1 + m_3 = 0$) and

https://doi.org/10.1017/S0022112003004816 Published online by Cambridge University Press

$h_4 = 0.17\ldots$ (point H_4, $m_2 = 0$). Some remarks on which types of steady-state waves are expected for those critical depths will be made below. However, since a two-dimensional sloshing model assuming a single dominant $\beta_{1,0}$ has limited applicability for those depths with increasing forcing, these conclusions are of a preliminary character and a series of special studies is required to describe quantitatively both the passage from finite to shallow depths and from extremely small to larger forcing amplitudes as done by Faltinsen & Timokha (2001) and Faltinsen & Timokha (2002*a*) for 'planar' resonant sloshing.

Taking into account (3.12), multiplying the first and second equations of (3.10) by $\bar{A}$ and A respectively and subtracting the resulting equations gives

$$(m_2 - m_3)\left[A\bar{A}(\bar{B}^2 - B^2) + B\bar{B}(\bar{A}^2 - A^2)\right] = P_1\bar{A}. \tag{3.17}$$

Proceeding in a similar way with the third and fourth equations by multiplying by B and $\bar{B}$ respectively yields

$$(m_2 - m_3)\left[A\bar{A}(\bar{B}^2 - B^2) + B\bar{B}(\bar{A}^2 - A^2)\right] = 0. \tag{3.18}$$

The graphs of $m_i(h, \sigma_1)$ in figure 4 confirm that $m_2 - m_3 \neq 0$ under resonance condition $\sigma \approx \sigma_1$. Since $P_1 \neq 0$ and (3.17), (3.18) have equal left-hand sides, we deduce that $\bar{A} = 0$. Substituting $\bar{A} = 0$ into (3.18) and using the first equation of (3.10) gives the following solvability condition of the system (3.10):

$$\bar{A} = 0, \quad A \neq 0, \quad B\bar{B} = 0. \tag{3.19}$$

This solvability condition yields three, and only three, possible solutions of (3.10), for which the amplitude A of the directly excited mode $f_1^{(1)}$ is always non-zero. Corresponding steady-state waves are

(i) 'planar'

$$f(x, y, t) = Af_1^{(1)}(x)\cos\sigma t + o(\epsilon^{1/3}), \tag{3.20}$$

occurring when $A \neq 0$ and $\bar{A} = B = \bar{B} = 0$,

(ii) 'square'-like

$$\begin{aligned} f(x, y, t) &= \left[Af_1^{(1)}(x) \pm \bar{B}f_1^{(2)}(y)\right]\cos\sigma t + o(\epsilon^{1/3}) \\ &= \left[A_1^{\pm}\underbrace{\left(f_1^{(1)}(x) - f_1^{(2)}(y)\right)}_{S_1^1(x,y)} + B_1^{\pm}\underbrace{\left(f_1^{(1)}(x) + f_1^{(2)}(y)\right)}_{S_2^1(x,y)}\right]\cos\sigma t + o(\epsilon^{1/3}) \end{aligned} \tag{3.21}$$

occurring for $A \neq 0$ and $\bar{A} = B = 0$, $\bar{B} \neq 0$, and, finally,

(iii) 'swirling'

$$f(x, y, t) = Af_1^{(1)}(x)\cos\sigma t \pm Bf_1^{(2)}(y)\sin\sigma t + o(\epsilon^{1/3}) \tag{3.22}$$

occurring for $A \neq 0$ and $B \neq 0$, $\bar{B} = \bar{A} = 0$. The reason why (3.22) describes 'swirling' is that the x- and y-dependent terms are 90° out of phase. The $\pm$ in front of the amplitude component B in (3.22) means clockwise or counterclockwise 'rotation'. Since a 'square'-like wave corresponds to a nearly diagonal standing wave, $\pm$ in (3.21) describes the possibility that the waves can occur approximately along either of the two diagonals. Both signs are mathematically possible. This means that initial conditions and transient phase will determine the sign.

https://doi.org/10.1017/S0022112003004816 Published online by Cambridge University Press

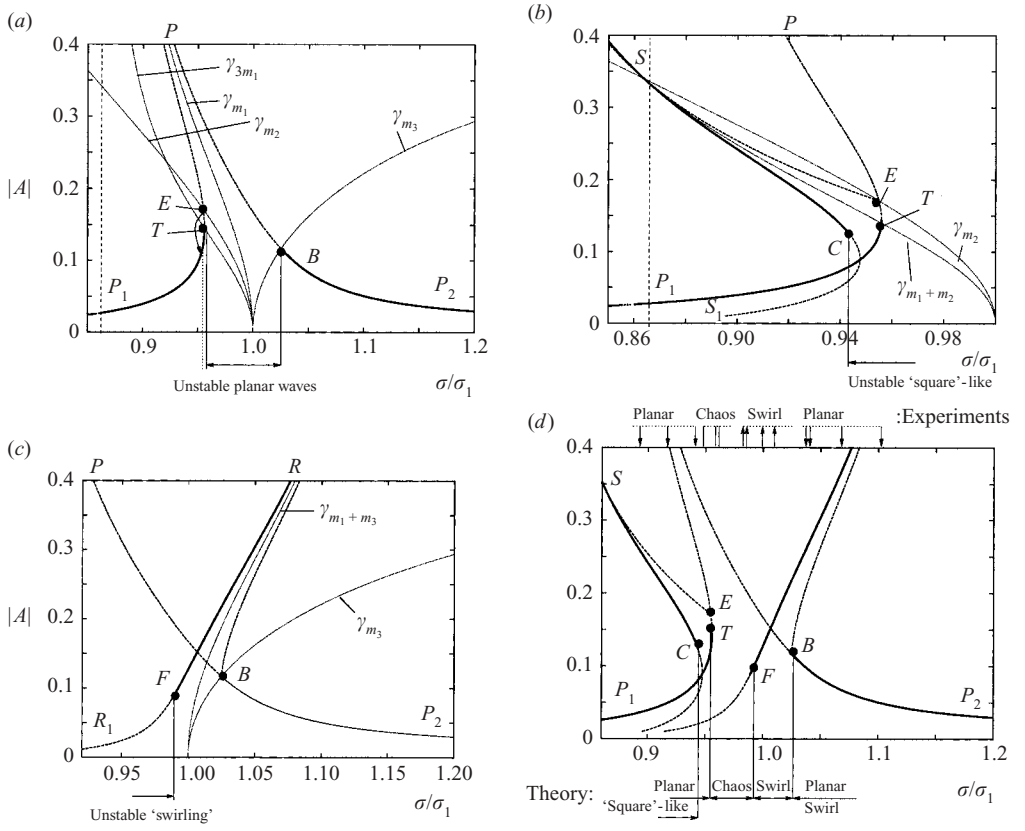


FIGURE 5. Steady-state wave amplitude response A of a_1 due to horizontal excitation along the Ox-axis versus σ/σ_1. The calculations were made for $h = 0.508$ and $H = 0.0078$ related to our model tests. Bold solid lines denote the stable steady-state motions. The secondary resonance by the secondary modes a_1 and b_1 (condition $\sigma_{2,0} = 2\sigma$) is estimated at $\sigma/\sigma_1 = i_2 = 0.737\ldots$. The secondary resonance by the mode c_{11} (condition $\sigma_{1,1} = 2\sigma$) occurs at $\sigma/\sigma_1 = i_{11} = 0.6136\ldots$. The coefficient $m_1(0.508, \sigma)$ becomes zero at $\sigma/\sigma_1 = 0.867\ldots$. (*a*) The response of the 'planar' motions (branches P_1P and PP_2). They are unstable between the pairs of the auxiliary curves $\gamma_{m_1}, \gamma_{3m_1}$ and $\gamma_{m_2}, \gamma_{m_3}$. For $h > h_5$ this unstable zone is defined by the ordinates of T and B. Since $m_2 < 3m_3$ for $h < h_5$, the left bound will then be defined by the ordinate of E and the corresponding stable sub-branch becomes P_1E. (*b*) Steady-state wave amplitude response of the 'square'-like waves (3.21) represented by the component A (branches S_1S and SE). (*c*) The amplitude component A for 'swirling' waves (branches R_1R and RB). (*d*) The final representation of stable and unstable periodic solutions and compares it with experimental observations.

Since $A \neq 0$ for all the steady-state solutions (i)–(iii), we can in the following treat the amplitude response of the periodic solutions in the $(\sigma/\sigma_1, |A|)$-plane. An example for $h = 0.508$, $H = 0.0078$ (related to our model tests) is presented in figure 5(*a–d*).

The 'planar' waves (3.20) were recently re-examined by Faltinsen *et al.* (2000) by means of a similar modal technique. It related the analysis to the single secular equation

$$A\left(\left(\bar{\sigma}_1^2 - 1\right) + m_1 A^2\right) = P_1. \tag{3.23}$$

This equation defines two branches in the $(\sigma/\sigma_1, |A|)$-plane, which have 'soft/hard' spring behaviour for $(h > h_1)/(h < h_1)$ respectively. A typical 'soft'-like response is

https://doi.org/10.1017/S0022112003004816 Published online by Cambridge University Press

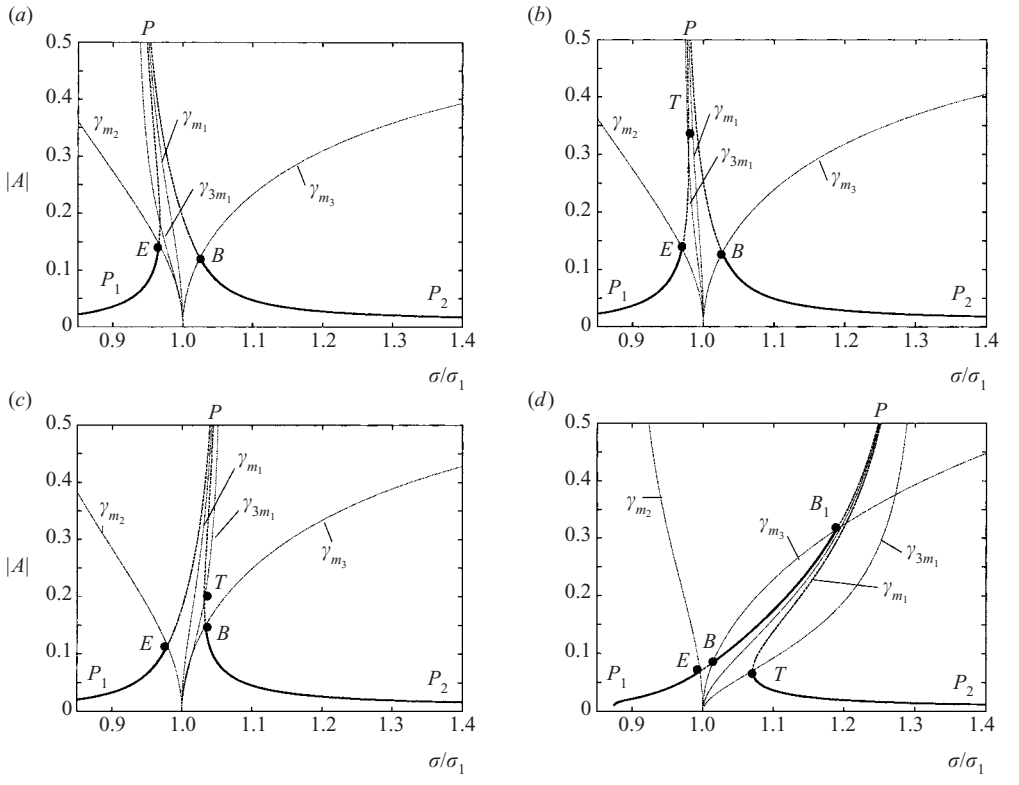


FIGURE 6. The steady-state 'planar' wave amplitude response $(\sigma/\sigma_1, A)$ versus h. Horizontal excitation along the Ox-axis with $H = 0.0078$. Bold solid lines denote stable steady-state 'planar' sloshing. Secondary resonance conditions are defined in figure 5. (*a*) $h = 0.4$ with $i_2 = 0.762, i_{11} = 0.627$ and $m_1(0.4, \sigma) = 0$ for $\sigma/\sigma_1 = 0.93$; (*b*) $h_1 < h < h_5$ (calculations were made for $h = 0.36$ with $i_2 = 0.7766, i_{11} = 0.63371$ and $m_1(0.36, \sigma) = 0$ for $\sigma/\sigma_1 = 0.970762$); (*c*) $h_2 < h < h_1$ (calculations were made for $h = 0.3$ with $i_2 = 0.80524, i_{11} = 0.6463$ and $m_1(0.3, \sigma) = 0$ for $\sigma/\sigma_1 = 1.0576$); (*d*) $h_4 < h < h_2$ (calculations were made for $h = 0.2$ with $i_{20} = 0.87366, i_{11} = 0.67171$ and $m_1(0.2, \sigma) = 0$ for $\sigma/\sigma_1 = 1.312635$).

demonstrated in figure 5(*a*). Solutions of (3.23) are illustrated by two branches P_1P and P_2P meeting each other at infinity. Faltinsen (1974) established that solutions exhibited by those branches are unstable between two auxiliary curves $\gamma_{m_1} : \bar{\sigma}_1^2 - 1 + m_1A^2 = 0$ and $\gamma_{3m_1} : \bar{\sigma}_1^2 - 1 + 3m_1A^2 = 0$ with the turning point T the intersection point of γ_{m_2} and P_1P. However, this analysis assumed only two-dimensional perturbations. Considering stability condition (3.16) one finds analytically an additional unstable zone between the two other auxiliary curves $\gamma_{m_2} : \bar{\sigma}_1^2 - 1 + m_2A^2 = 0$ and $\gamma_{m_3} : \bar{\sigma}_1^2 - 1 + m_3A^2 = 0$. Figure 4 shows that $m_3 > 0$ for all the depths, while m_2 changes sign at $h_4 = 0.17\ldots$. This means that the curve γ_{m_3} always demonstrates a 'hard'-like behaviour and intersects the branch P_2P at the point B. The curve γ_{m_2} has instead for $h < h_4$ a 'soft'-like character. In addition, it is situated between γ_{m_1} and γ_{3m_1} for $h > h_5$ and lies under γ_{3m_1} for $h < h_5$, where h_5 is associated with the condition $3m_1 = m_2$ (point E in figure 4). This means that for $h > h_5$ the stable planar steady regimes are associated with the sub-branches P_1T and BP_2. If $h_4 < h < h_5$, E is left of T and the left-hand stable sub-branch is P_1E. Note that a similar modal analysis of 'planar' sloshing in vertical circular cylindrical tanks gives an unstable zone between T and B (see Miles 1984*a*, *b* and Gavrilyuk *et al.* 2000). Figure 6(*a–d*) presents the

https://doi.org/10.1017/S0022112003004816 Published online by Cambridge University Press

evolutions of 'planar' response versus the mean depth and show the characteristic behaviour as previously discussed.

We would again like to stress that our modal technique uses the dependence of m_i on σ. This means that some of the functions m_i or some of their linear combinations may become zero for depths close but not equal to the critical depths h_j for a small difference between σ and σ_1. Further, even if we consider a critical depth h_i, the corresponding m_i or their linear combinations become non-zero away from σ_1. This point was extensively discussed by Faltinsen *et al.* (2000) for two-dimensional sloshing. The calculations made for the depths in figure 5(*a*) gave the critical value $\sigma/\sigma_1 = 0.867$ where $m_1(0.508, \sigma/\sigma_1) = 0$.

Conditions $\bar{A} = B = 0$, $A \neq 0$, $\bar{B} \neq 0$ eliminate two equations of the system (3.10). The remaining pair needs the additional solvability condition

$$m_1 \neq m_2, \quad m_1 \neq 0. \tag{3.24}$$

Taking into account the numerical data in figure 4 we see that (3.24) fails only in a small vicinity of h_1 for $\sigma \approx \sigma_1$. This reduces (3.10), (3.12) to the following form:

$$A\left[\left(\bar{\sigma}_1^2 - 1\right) + (m_1 + m_2)A^2\right] = \frac{m_1}{m_1 - m_2} P_1, \quad \bar{B}^2 = -\left(m_2 A^2 + \left(\bar{\sigma}_1^2 - 1\right)\right)/m_1 \geqslant 0. \tag{3.25}$$

Figure 5(*b*) gives the 'square'-like wave amplitude response $|A|$ of the primary mode $f_1^{(1)}$ for $h = 0.508$ (solution (ii)). Since $m_1, m_2 < 0$ for this depth and only real $\bar{B}$ has a physical meaning, the inequality in (3.25) indicates that the solutions can appear only under the auxiliary curve γ_{m_2}. Calculations establish the unstable sub-branch ES emerging from E (the bifurcation point between solutions (3.20) and (3.21)). The branch SS_1 is divided by the point C (Hopf bifurcation) into stable and unstable subsets. A qualitative picture of which branches are expected for smaller depths $h < h_1$ is shown in figure 7(*a–d*).

Conditions $\bar{A} = \bar{B} = 0$, $A \neq 0$, $B \neq 0$ lead to a system of two equations needing the solvability condition

$$m_1 \neq m_3 \quad \text{and} \quad m_1 \neq 0. \tag{3.26}$$

This means that the third-order modal analysis may fail near h_1 and h_2 (figure 4). Under conditions (3.26) the secular system takes the form

$$A\left[\left(\bar{\sigma}_1^2 - 1\right) + (m_1 + m_3)A^2\right] = m_1 P_1/(m_1 - m_3), \quad B^2 = -\left(m_3 A^2 + \left(\bar{\sigma}_1^2 - 1\right)\right)/m_1 \geqslant 0. \tag{3.27}$$

A typical 'swirling'-like wave response of A versus σ/σ_1 is shown in figure 5(*c*) for $h = 0.508$. It establishes the bifurcation point B defined by the intersection of γ_{m_3} and the branch PP_1 corresponding to the 'planar' response. However, corresponding branch BR is unstable (as for a vertical circular cylinder, see Miles 1984*b* or Gavrilyuk *et al.* (2000). Figure 8(*a–d*) illustrates how the 'swirling' response changes with decreasing h. The results show that 'swirling' may become impossible for sufficiently small h, because its effective domain undergoes an upshift away from the main resonance, where the steady-state 'planar' wave of lower amplitude exists.

Finally, figures 5(*d*) and 9 include all the stable branches for $h = 0.508$ and 0.34. Since $h = 0.34 \approx h_1$ in the case of figure 9, m_1 may become zero near $\sigma/\sigma_1 = 1$ and therefore one of the solvability conditions is not fulfilled there, and the theory may give wrong predictions in a very small vicinity of the main resonance, where theoretical prediction in figure 9 indicates possible irregular waves.

https://doi.org/10.1017/S0022112003004816 Published online by Cambridge University Press

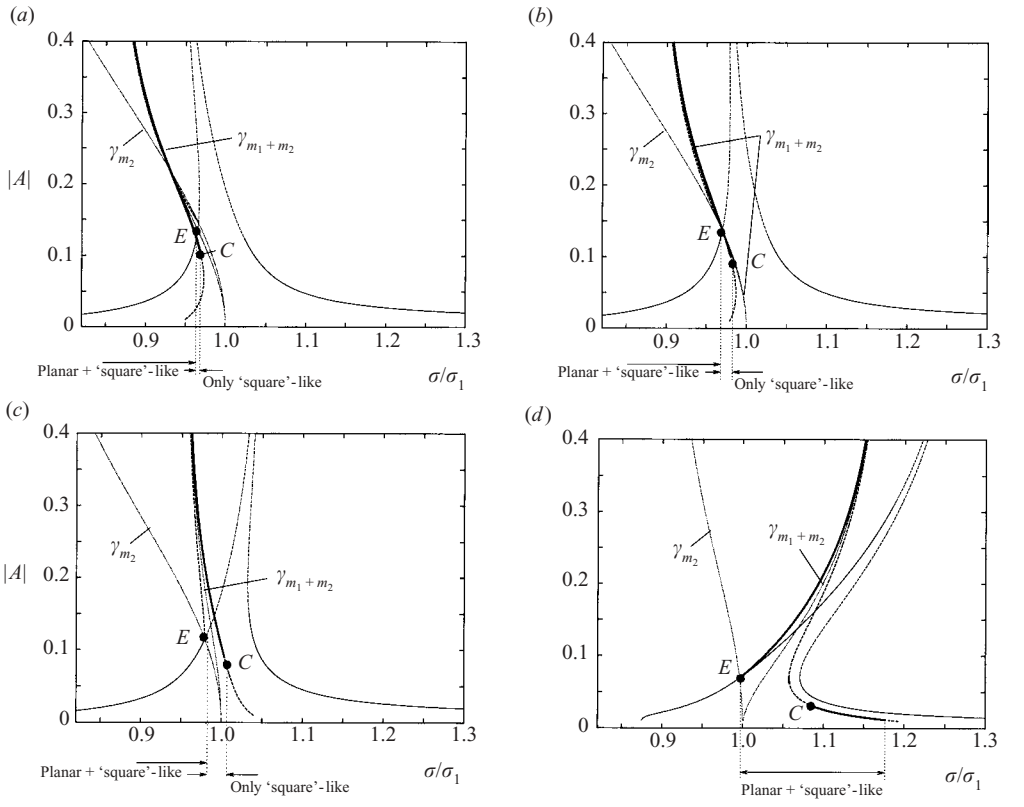


FIGURE 7. The steady-state wave amplitude component A of 'square'-like waves versus σ/σ_1 for different h. Horizontal excitation along the Ox-axis with $H = 0.0078$. (*a–d*) The same fluid depths as in figure 6(*a–d*). Solid thin lines denote stable 'planar'-waves, while bold solid lines imply stable 'square'-like waves. The figures demonstrate that 'square'-like waves become the most important for small depths ($h < h_3 = 0.27\ldots$).

The change with h of the frequency domains for the steady-state solutions is summarized in figure 10. It shows that the frequency domain of chaotic (irregular) waves vanishes with decreasing h. Figure 11 demonstrates that the frequency domain where three-dimensional phenomena are expected increases with the excitation amplitude and resonant 'planar' waves will probably disappear for a critical amplitude.

3.5. *Steady-state resonant sloshing due to diagonal excitation* ($r = 1,\ P_1 = P_2 \neq 0$)

Assuming $P_1 = P_2 \neq 0$ the analytical computations of the previous subsection applied to (3.10) gives the auxiliary equality (3.17) together with

$$(m_2 - m_3)\left[A\bar{A}(\bar{B}^2 - B^2) + B\bar{B}(\bar{A}^2 - A^2)\right] = BP_1. \tag{3.28}$$

Under the already mentioned inequality $m_2 \neq m_3$ equations (3.17) and (3.28) lead to the following solvability condition of (3.10):

$$B = -\bar{A}, \quad (m_1 - m_3)B(\bar{B}^2 - A^2) = 0. \tag{3.29}$$

When $m_1 \neq m_3$ (figure 4 shows that equality $m_1 = m_3$ is fulfilled only at an isolated depth $h_2 = 0.274\ldots$) the solvability condition (3.29) defines, three and only three, periodic resonant waves. We find it convenient to present them in the terms of 'square' modes, i.e.

https://doi.org/10.1017/S0022112003004816 Published online by Cambridge University Press

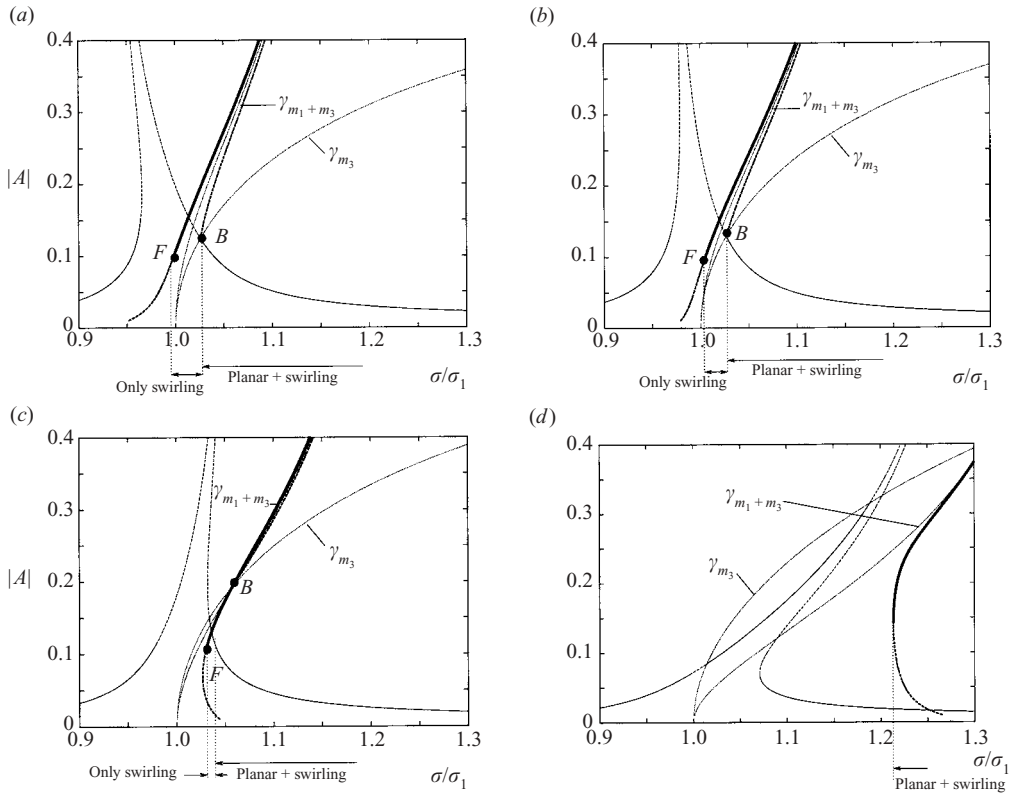


FIGURE 8. The steady-state wave amplitude component A of 'swirling' waves versus σ/σ_1 for different h. Horizontal excitation along the Ox-axis with $H = 0.0078$. (a–d) The same fluid depths as in figure 6(a–d). Solid thin lines denote stable sub-branches for 'planar' and 'square'-like waves and bold solid lines imply stable 'swirling' waves motions. The figure shows upshift of the frequency domain for 'swirling' waves away of the main resonance range with decreasing fluid depth.

(i) 'diagonal' waves (pure 'square' mode $S_2^1(x, y)$ to be nonlinearly excited)

$$f = B_1 S_2^1(x, y)\cos\sigma t + o\left(\epsilon^{1/3}\right) \tag{3.30}$$

occurring for $B = -\bar{A} = 0,\ A = \bar{B} \stackrel{def}{=} B_1$,
(ii) 'square'-like waves

$$f = \left[\pm A_1 S_1^1(x, y) + B_1 S_2^1(x, y)\right]\cos\sigma t + o\left(\epsilon^{1/3}\right) \tag{3.31}$$

describing joint cosine amplification of the pair S_1^1 and S_2^1 (here $B_1 \stackrel{def}{=} (A+\bar{B})/2,\ A_1 \stackrel{def}{=} (A-\bar{B})/2$) occurring for $B = -\bar{A} = 0$, $A \neq \bar{B}$, and, finally
(iii) 'swirling' waves

$$f = B_1 S_2^1(x, y)\cos\sigma t \mp A_1 S_1^1(x, y)\sin\sigma t + o(\epsilon^{1/3}) \tag{3.32}$$

occurring for $A_1 \stackrel{def}{=} \bar{A} = -B \neq 0,\ B_1 \stackrel{def}{=} A = \bar{B}$.

Periodically forced mode S_2^1 emerges as a necessary component of the solutions (i)–(iii) and therefore $B_1 \neq 0$. This point enables us to treat the nonlinear response in the $(\sigma/\sigma_1, |B_1|)$-plane. The analysis below is mathematically equivalent to the

https://doi.org/10.1017/S0022112003004816 Published online by Cambridge University Press

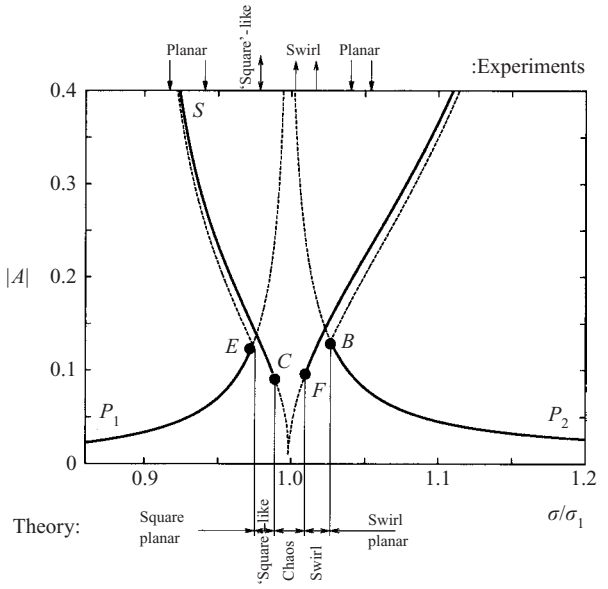


FIGURE 9. Comparisons between experimental observations and theoretical predictions of different types of stable periodic (steady-state) wave motions. Longitudinal excitations with $h = 0.34$, $H = 0.0078$. Theoretical results and experimental classification are presented on the bottom and top respectively.

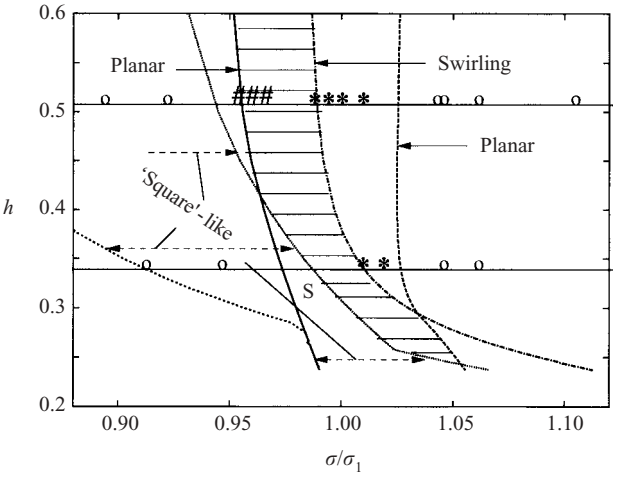


FIGURE 10. Theoretical ranges of stable steady-state motions for different h. Horizontal excitation along the Ox-axis with $H = 0.0078$. Shaded area indicates no stable steady-state solutions. It vanishes for $h < 0.25$. Results of experimental observations are given for $h = 0.508$ and 0.34. ○, 'planar' waves; ∗, 'swirling'; #, irregular motions; and S, 'square'-like waves.

corresponding scheme described for longitudinally excited steady-state sloshing, and so we will not present the details.

'Diagonal' waves (3.30) ($B = -\bar{A} = 0,\ A = \bar{B} = B_1$) are calculated from the single secular equation

$$B_1\left(\bar{\sigma}_1^2 - 1 + (m_1 + m_2)B_1^2\right) = P_1 \tag{3.33}$$

https://doi.org/10.1017/S0022112003004816 Published online by Cambridge University Press

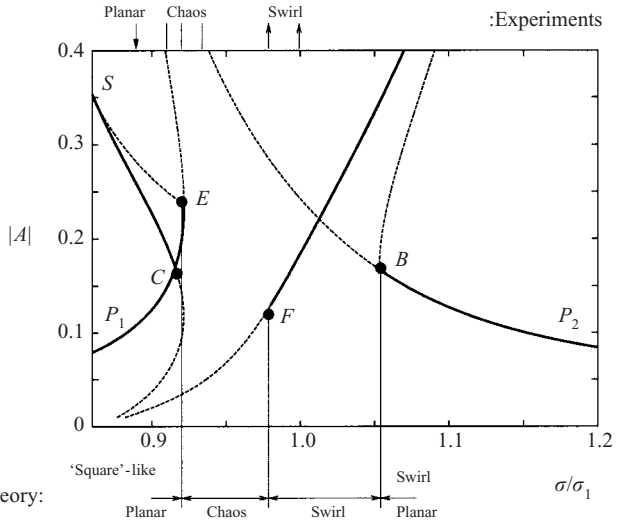


FIGURE 11. Comparisons between experimental observations and theoretical predictions of different types of stable periodical (steady-state) wave motions. Longitudinal excitations with $h = 0.508$, $H = 0.025$.

governing the amplitude of S_2^1 (see (3.30)). Since $m_1 + m_2$ changes sign at $h = h_3$ (see figure 4), corresponding branches in the $(\sigma/\sigma_1, |B_1|)$-plane imply 'soft'-like spring behaviour for $h > h_3$ and 'hard'-like spring behaviour for $h < h_3$. Branches D_1D and DD_2 in figures 12(a,b) exemplify this response for two depths ($h = 0.508$ and 0.34) related to our experimental series. It can be shown analytically that corresponding steady-state solutions become unstable for the segments of these branches lying between pairs of auxiliary curves $\gamma_{m_1+m_2}$, $\gamma_{3(m_1+m_2)}$ and $\gamma_{3m_1-m_2}$, $\gamma_{m_1-m_2+m_3}$ defined by the equations $\bar\sigma_1^2 - 1 + (m_1+m_2)B_1^2 = 0$, $\bar\sigma_1^2 - 1 + 3(m_1+m_2)B_1^2 = 0$, $\bar\sigma_1^2 - 1 + (3m_1 - m_2)B_1^2 = 0$ and $\bar\sigma_1^2 - 1 + (m_1 - m_2 + 2m_3)B_1^2 = 0$ respectively. These curves intersect the branches at the turning point T and the two Poincaré-bifurcation points E and B, which originate from the wave solutions (3.31) and (3.32), respectively.

'Square'-like waves (3.31) appear with $B = -\bar A = 0$, $A \neq \bar B$. Taking into account that $A = A_1 + B_1$, $\bar B = B_1 - A_1$ reduces the secular system (3.29) to the form

$$\left.\begin{aligned} B_1\left(\bar\sigma_1^2 - 1 + (m_1+m_2)B_1^2 + (3m_1 - m_2)A_1^2\right) &= P_1, \\ \bar\sigma_1^2 - 1 + (m_1+m_2)A_1^2 + (3m_1 - m_2)B_1^2 &= 0. \end{aligned}\right\} \tag{3.34}$$

This system needs the solvability condition

$$m_1 + m_2 \neq 0, \quad m_1 \neq m_2, \tag{3.35}$$

which is not satisfied except for two isolated depths $h = h_2$ and h_3 (figure 4). If (3.35) is satisfied, the system (3.34) can be re-written as

$$\left.\begin{aligned} B_1\left(\bar\sigma_1^2 - 1 + 4m_1B_1^2\right) &= P_1\frac{m_1+m_2}{2(m_2-m_1)}, \\ A_1^2 &= -\left(\bar\sigma_1^2 - 1 + (3m_1 - m_2)B_1^2\right)/(m_1+m_2) \geqslant 0. \end{aligned}\right\} \tag{3.36}$$

The system (3.36) defines the pair of conjugated solutions $B_1, \pm A_1$, where $\pm$ are associated with two Oy-symmetric directions. Calculations performed for various depths from $h = 1$ to $h = 0.15$ showed that (ii) is always unstable. However, we

https://doi.org/10.1017/S0022112003004816 Published online by Cambridge University Press

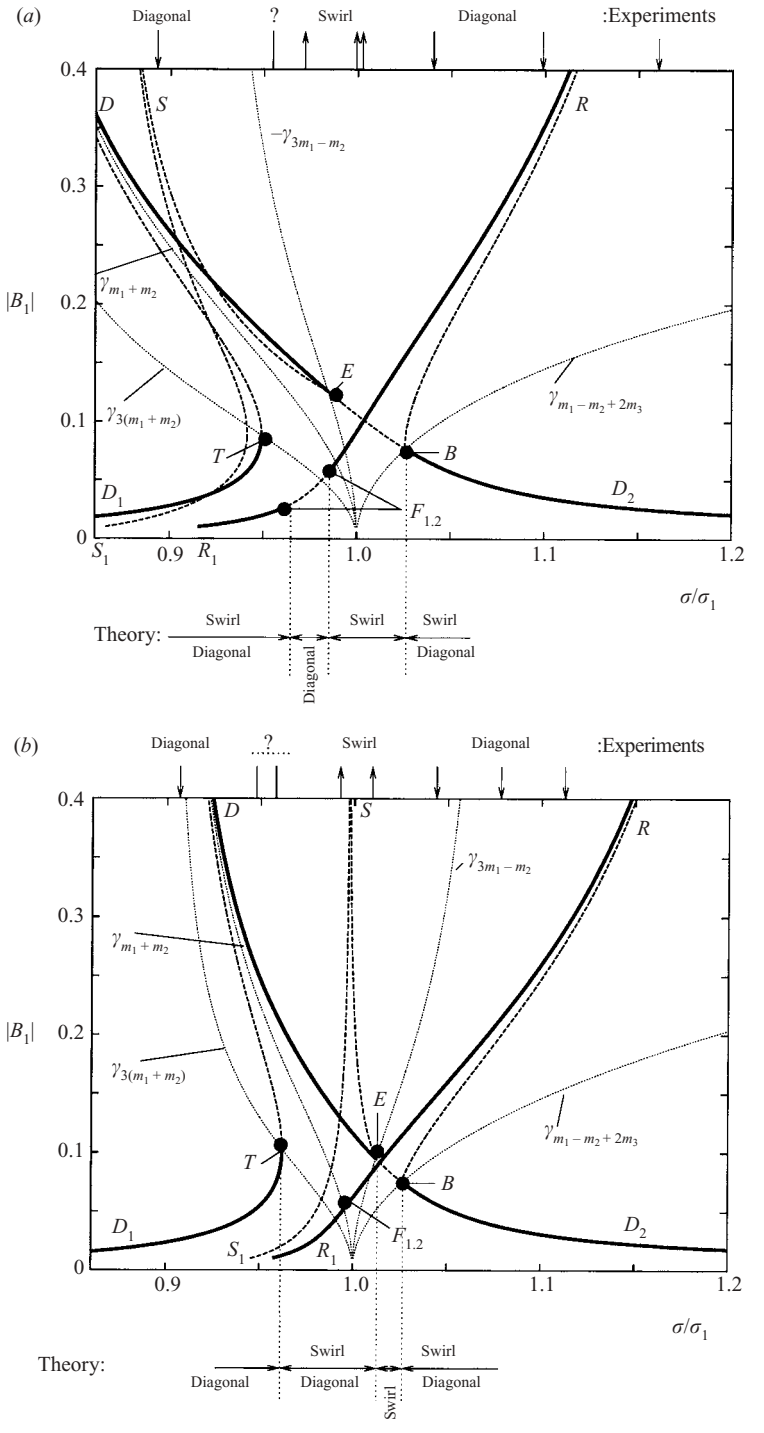


FIGURE 12. The steady-state wave amplitude response B_1 versus σ/σ_1 for diagonal forcing and $H = 0.0078$. Three alternative solutions are denoted as branches D_1DD_2 ('diagonal' wave), S_1SE ('square'-like waves) and R_1RB ('swirling' waves). Bold solid lines denote stable sub-branch. (*a*) $h = 0.508$; (*b*) case $h = 0.34$. Theoretical results and experimental classification of the types of wave motions are presented on the bottom and the top respectively.

https://doi.org/10.1017/S0022112003004816 Published online by Cambridge University Press

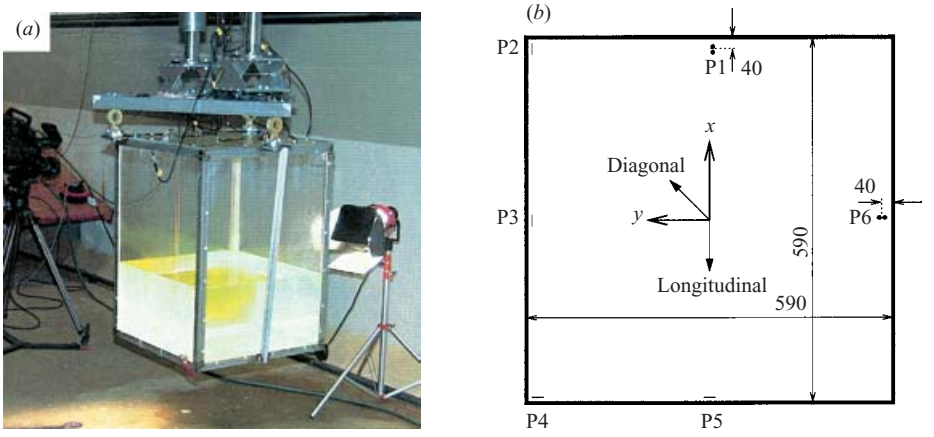


FIGURE 13. (*a*) A photo of the experimental setup and (*b*) the top view of the tank with positions of the wave probes. All the dimensions in mm.

present the corresponding branches S_1S and SE in figure 12(*a*, *b*). Here E is the Poincaré bifurcation point between 'diagonal' and 'square'-like waves.

'Swirling' waves (3.32) ($\bar{A} = -B \neq 0$, $A = \bar{B}$) are governed by the system

$$\left.\begin{aligned} &B_1\left(\bar{\sigma}_1^2 - 1 + (m_1 + m_2)B_1^2 + (m_1 - m_2 + 2m_3)A_1^2\right) = P_1, \\ &\bar{\sigma}_1^2 - 1 + (m_1 + m_2)A_1^2 + (m_1 - m_2 + 2m_3)B_1^2 = 0 \end{aligned}\right\} \tag{3.37}$$

under the solvability condition

$$m_1 + m_2 \neq 0, \quad m_2 \neq m_3.$$

This condition excludes from the consideration the isolated critical depth h_3 (figure 4) where $m_1 + m_2 = 0$ and reduces (3.37) to the form

$$\left.\begin{aligned} &B_1\left(\bar{\sigma}_1^2 - 1 + 2(m_1 + m_3)B_1^2\right) = \frac{m_1 + m_2}{2(m_2 - m_3)}P_1, \\ &A_1^2 = -\left(\bar{\sigma}_1^2 - 1 + (m_1 - m_2 + 2m_3)B_1^2\right)/(m_1 + m_2) \geqslant 0 \end{aligned}\right\} \tag{3.38}$$

It has also the pair of conjugated solutions $B_1, \pm A_1$, where plus or minus mean physically clockwise/counterclockwise 'rotation'. The amplitude component B_1 versus σ/σ_1 is represented in figures 12(*a*, *b*) by the branches BR and RR_1. Stability analysis shows numerically two Hopf bifurcations on the branch RR_1, denoted as F_1 and F_2, when $h > h_1$. 'Swirling' waves corresponding to solutions between these points become unstable. This instability zone disappears for $h < h_1$ and therefore F_1 coincides with F_2 at $h = h_1$ as shown in figure 12(*b*). Numerical examination of the case in figure 12(*a*) establishes that probably a small dissipation here can eliminate (or dramatically reduce) the instability between F_1 and F_2. The reason is that computed $c_1^2 - 4c_0$ is of order 10^{-6} in this range.

4. Model tests

4.1. *Setup and observations*

We conducted a series of model tests on resonant sloshing with the aim of classifying all the possible nonlinear wave motions. Both video recordings and actual measurements were performed. A photo of the setup is presented in figure 13(*a*).

https://doi.org/10.1017/S0022112003004816 Published online by Cambridge University Press

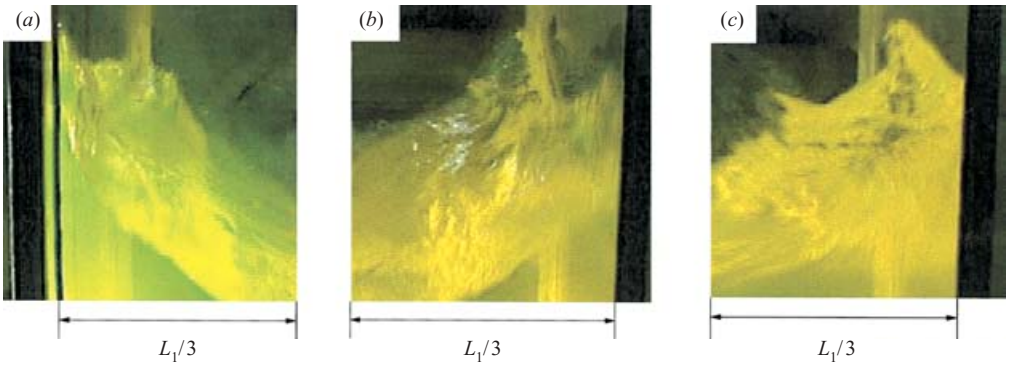


FIGURE 14. Photos from the experimental series demonstrating local phenomena near the wall occurring for three-dimensional waves. Actual width of the photos is approximately 1/3 of the tank length L_1.

The tank had a square base with breadth/width 59 cm and a height of 80 cm. The tank height was sufficiently large to avoid tank roof impact due to sloshing in the series documented. It was ensured that the walls and bottom of the tank were stiff enough to avoid hydroelastic effects. Fresh water was used. The non-dimensional water depths (depth/breath ratio) were $h = 0.508$ (related to $h = 0.5$ in Chen & Arai 1995), $h = 0.34$ (near the critical depth for the 'planar' waves and $h = 0.27$ (near an artificial bound for the applicability of the single dominant theory of two-dimensional sloshing established by Faltinsen *et al.* (2000)). Some isolated tests were made with other depths. The setup allowed changes in the excitation direction. Most experiments were for horizontal longitudinal (along the Ox-axis) and diagonal excitations as indicated on the top view in figure 13(*b*). The typical excitation amplitude was about 0.5 cm. This gives dimensionless $H = 0.0078$ for longitudinal forcing and $H_1 = 0.0078/\sqrt{2}$, $H_2 = 0.0078/\sqrt{2}$ for diagonal excitations, where H_i are defined by (3.6). A few measurements were made with higher forcing amplitudes. The wave probes 1–6 were of two different types (figure 13*b*). Probes 1 and 6 are made of thin wires with 0.5 mm diameter and placed a distance 40 mm from the wall. The experimental error due to meniscus effects for wave probes 1 and 6 is less than 1 mm. The other probes are made of copper tape. They are placed directly on the tank walls and have a total width of approximately 20 mm. Since experiments were done prior to the theoretical studies and the authors were not familiar with possible theoretical predictions, the test series were for a wide range of excitation frequencies in the vicinity of primary resonance ($0.86 < \sigma/\sigma_1 < 1.08$).

Visual observations and video recordings always showed three-dimensional waves in the small vicinity of the lowest natural frequency. Two-dimensional/diagonal sloshing was observed for longitudinal/diagonal excitation when the forcing frequency was outside this frequency domain. The experiments lasted for about 120 forcing periods and clear steady-state regimes were not achieved even for this long series. The transient behaviour during the first 80 s changed between being dominated by 'planar'/'diagonal', 'square' and 'swirling' wave modes. This long transient behaviour was observed earlier for two-dimensional sloshing by Faltinsen *et al.* (2000). The reason is very small dissipation. The wave profiles were particularly steep near the corners and, although the forcing amplitude was sufficiently small, all the three-dimensional waves demonstrated significant local near-wall phenomena appearing as run-up at the walls accompanied by splashing/overturning with possible

https://doi.org/10.1017/S0022112003004816 Published online by Cambridge University Press

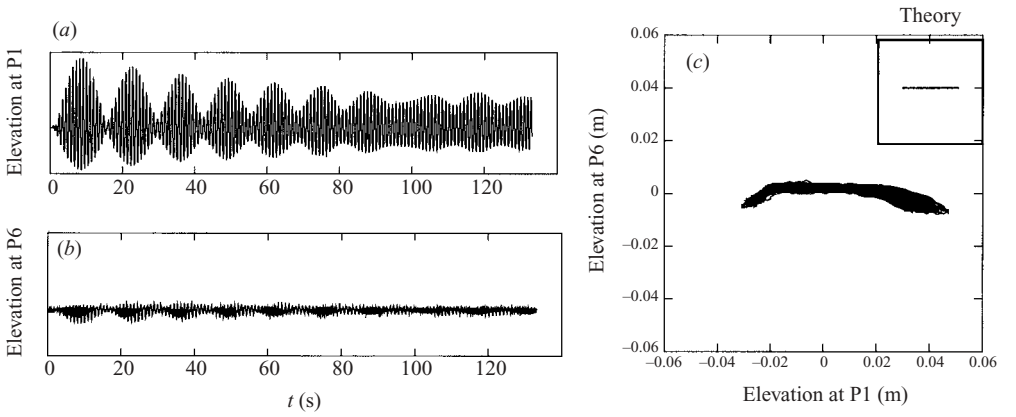


FIGURE 15. Example of measurements at the wave probes 1 and 6 and corresponding parametric curve ('measured probe 1'(t), 'measured probe 6'(t)) for 'planar' waves. The tank was longitudinally excited with $h = 0.508$, $H = 0.0078$ and $\sigma/\sigma_1 = 0.92$.

drop formation. Typical instantaneous wave shapes near the walls are shown in figure 14(a–c). The situation was very similar to the description by Abramson (1966) and recently by Royon *et al.* (2002) (for a vertical circular cylindrical tank).

4.2. *Classification by primary amplitudes*

The observed nonlinear phenomena have been classified by comparing the lowest-order theoretical predictions of steady-state resonant motions with video recordings and measurements. Due to the importance of transients, only the last 30–50 s of measurements might under certain circumstances be used to indicate what type of steady-state motion was achieved. Since video recordings demonstrated a significant run-up in terms of a thin film of water at the wall, only wave probes 1 and 6 placed at a small distance from the wall were involved in the analysis. Preliminary theoretical predictions are made in terms of the primary modes $f_1^{(1)}(x)$ and $f_1^{(2)}(y)$ (or $S_2^1(x, y)$ and $S_1^1(x, y)$) and asymptotic solutions (3.20), (3.21), (3.22) and (3.30), (3.31), (3.32) correct to $O(\epsilon^{1/3})$. The theory gives four possible scenarios for both types of excitations. The longitudinal excitations exhibit (a) 'planar' two-dimensional waves occurring in the plane of the horizontal excitation (solution (3.20)) exemplified in figure 15(a–c); (b) 'swirling' waves (the surface wave crest moves along the tank wallsclockwise or counterclockwise and the direction of its motion by changes 90° at the corner) governed by the solution (3.22) shown in figure 16(a–c); (c) irregular waves widely observed when either no appropriate stable steady-state solution for this excitations frequency exists or due to the actual transients being so long that we could not clearly distinguish possible steady-state solution, demonstrated in figure 17(a–c), and, finally, rare in observations (d) 'square'-like waves demonstrating nearly diagonal standing waves (governed by (3.21)) shown in figure 18(a, b). A similar classification can be used for diagonal excitation, but in this case 'planar' waves (3.20) are replaced by 'diagonal' motions governed by (3.30) and 'square'-like waves may not be seen because they are unstable. The examples in figure 15–18 are accompanied by symbolic theoretical curves, which represent theoretical predictions based on approximation correct to $O(\epsilon^{1/3})$ and compared with experiments in the ('measured probe 1'(t), 'measured probe 6'(t))-plane. According to this approximation we expect a horizontal interval

https://doi.org/10.1017/S0022112003004816 Published online by Cambridge University Press

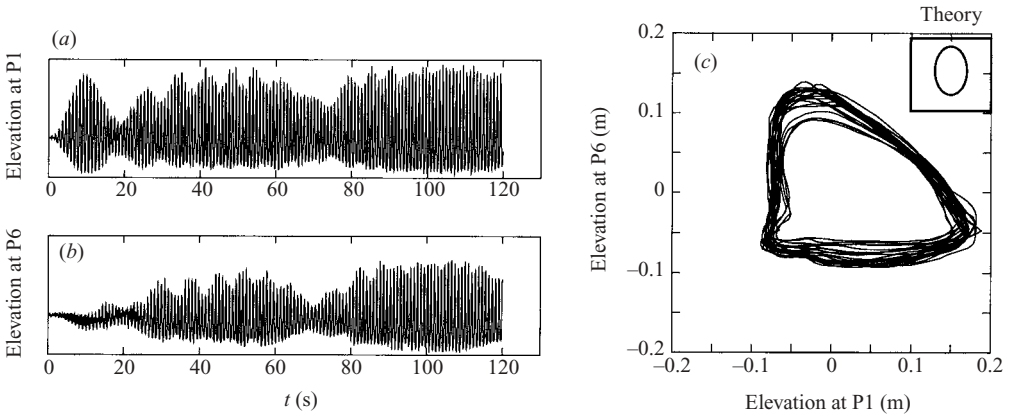


FIGURE 16. As figure 15 but for 'swirling' waves with $\sigma/\sigma_1 = 1.011$.

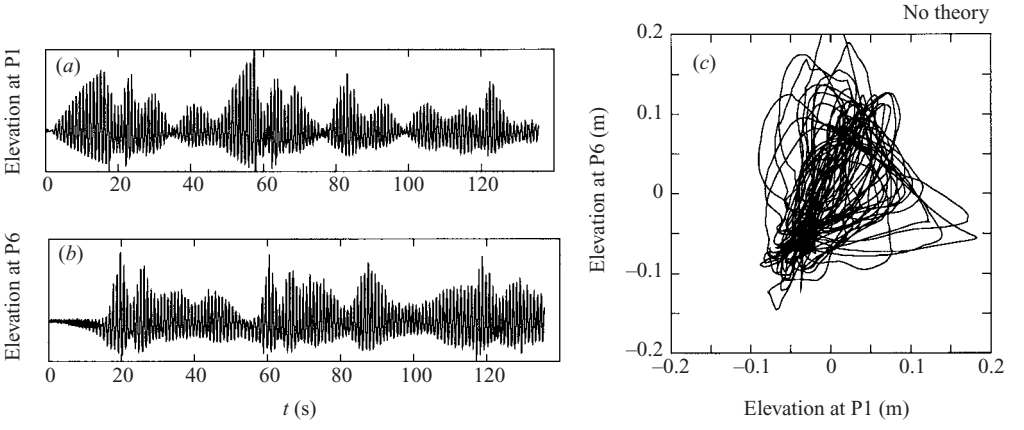


FIGURE 17. As figure 15 but for irregular waves with $\sigma/\sigma_1 = 0.945$.

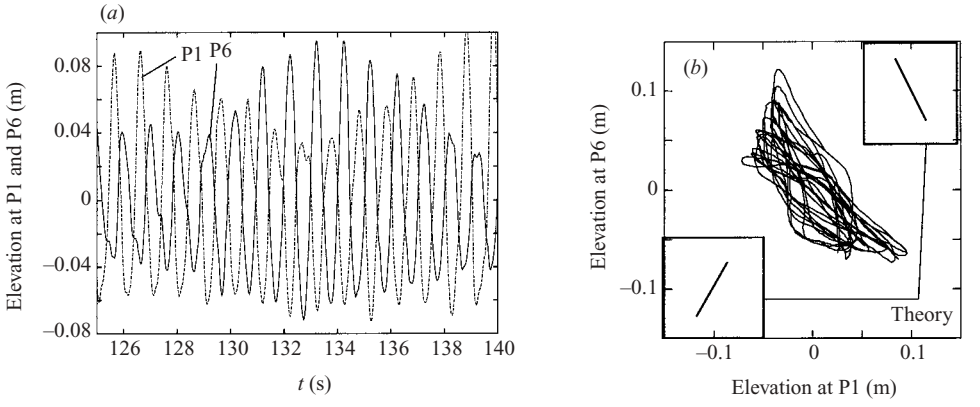


FIGURE 18. As figure 15 but for 'square'-like waves with $h = 0.34$, $\sigma/\sigma_1 = 0.98$.

https://doi.org/10.1017/S0022112003004816 Published online by Cambridge University Press

in the case of 'planar' motions (top right in figure 15(c)), an ellipse (the loop) for 'swirling' top right of figure 16(c) and an inclined interval for 'square'-like waves in the bottom left and top right of figure 18(c). No theoretical prediction exists for parametric curve in figure 17(c) for irregular motions.

The theoretical and experimental results for frequency domains of stable steady solutions for longitudinal excitation ($h = 0.508, H = 0.0078$) are shown on the bottom and the top of the $(\sigma/\sigma_1, |A|)$-plane in figure 5(d). The theory predicts for this case stable 'planar' and 'swirling' waves except when $0.955 \lesssim \sigma/\sigma_1 \lesssim 0.983$. No stable periodic solutions exist in this frequency domain and irregular oscillations are predicted. The figure shows good qualitative agreement between theory and experiments for the excitation amplitude $H = 0.0078$ as well as for larger excitation amplitude $H = 0.025$ in figure 11. Note that this increasing amplitude does not change qualitatively the distribution of the frequency domains for different types of wave motions. One should note that the theory for case $h = 0.508$ predicts stable 'square'-like waves to co-exist with 'planar' waves. Since the 'planar' solution has theoretically clearly the lowest amplitude and the experiments were for near-zero initial conditions, it is most probable that a 'square'-like wave was not physically realized in the experiments. Since the 'square'-like solutions are an attribute of lower depths, we were strongly motivated to find them in observations for $h = 0.34$. This depth is very close to the critical depth h_1, where $m_1 = 0$ and corresponding secular equations have no solutions. However, in our approximation m_1 is also a function of σ and $m_1(0.34, \sigma) \neq 0$ away from a small vicinity of σ_1. The theoretical predictions presented in figure 9 give a narrow zone near the main resonance where there is not any stable periodic solution. Since $m_1 \approx 0$ in this zone, it is understandable that the theoretical predictions may fail there. However, the theoretical and experimental predictions are in good agreement away from this range. As explained by Faltinsen & Timokha (2001) for two-dimensional sloshing, the discrepancy near $h = h_1, \sigma = \sigma_1$ can be corrected by accounting for secondary resonance effects. Only one experimental series at $\sigma/\sigma_1 = 0.98$ confirmed the existence of 'square'-like waves. Corresponding measured wave elevations are presented in figure 18(a, b). Additional work is required to provide more systematic studies of this phenomenon in the frequency domain indicated in figure 9.

We were also able to compare our theoretical results with experimental wave data for the diagonal excitations. The comparisons of experimental and theoretical results are presented in figure 12(a, b). There was generally good agreement except at the points denoted by '?' in the figures. These points corresponded to the case when the theory predicts two stable solutions, namely 'diagonal' and 'swirling' waves. The difference from the longitudinal excitation is that both solutions have comparable amplitudes in this zone (accounting for components A_1). While the 'diagonal' wave has a large component B_1^{diag}, the calculated values for 'swirling' waves give small contribution of B_1^{swirl}, but the corresponding A_1^{swirl} component is approximately equal to B_1^{diag}. This means that both types of periodical solutions are physically and mathematically possible when starting from a planar initial free-surface shape. The experimental measurements give regular 'beating' waves in this zone, exemplified in figure 19. We cannot, based on this, conclude which stable periodic solution will be realized from zero initial conditions. This would require a much larger time series. In addition, we cannot mathematically ignore possible stable steady-state aperiodic waves. Additional theoretical and experimental investigations of this phenomenon are needed.

https://doi.org/10.1017/S0022112003004816 Published online by Cambridge University Press

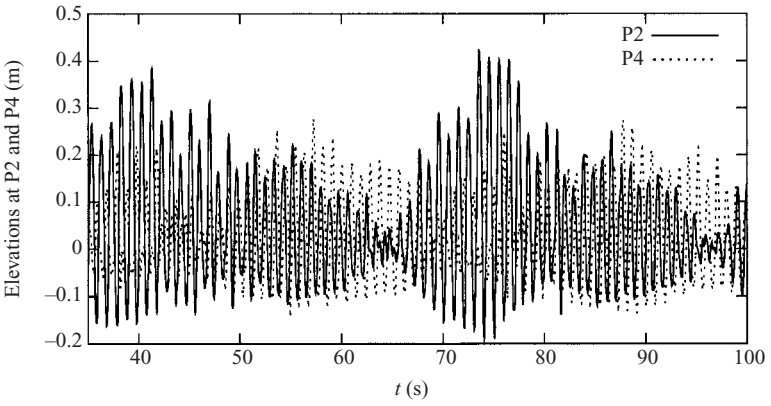


FIGURE 19. Two time series of the measured data at the wave probes 2 and 4, $h = 0.508$. The case in figure 12(a) with $\sigma/\sigma_1 = 0.9495$ labelled by '?'.

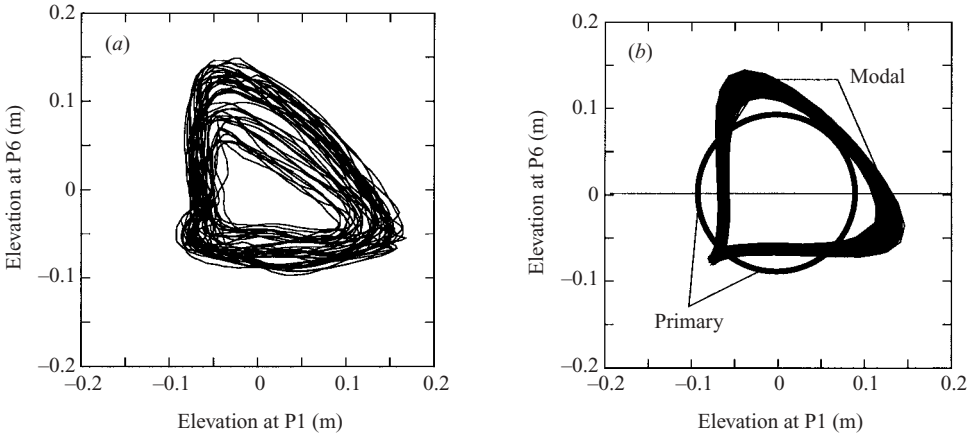


FIGURE 20. Comparisons between experimental and theoretical results for steady-state 'swirling' modes. Diagonal excitation $H = 0.0078$, $h = 0.508$, $\sigma/\sigma_1 = 1.008$. (a) The parametric graph from the experiments. (b) Theoretical predictions in the framework of primary modes $O(\epsilon^{1/3})$ ('Primary') and by the modal system (up to $O(\epsilon)$, 'Modal').

4.3. *Experimental validation of the modal system correct to* $O(\epsilon)$

Although none of the experimental series established clear periodic solutions, we made some effort to compare quantitatively the theoretical and experimental amplitudes. Our emphasis was on 'swirling' modes. The numerical technique uses the asymptotic approximation (3.8) to compute the appropriate initial conditions corresponding to periodic solutions of the modal system (3.3), (3.4). Since these initial conditions neglect the contribution of $o(\epsilon)$, the numerical integration by a Runge–Kutta method demonstrates a small beating effect. Some typical behaviours in the (Probe 1, Probe 6)-plane are shown in figures 20–22. Here parts (a) give experimental data and parts (b) present results by our calculations ('MODAL'). The elliptical curves 'PRIMARY' were drawn from predictions of leading modes. The figures confirm that although terms $o(\epsilon^{1/3})$ are formally small, they contribute in practice up to 60% of the wave response and make the modal method applicable for real simulations. This is

https://doi.org/10.1017/S0022112003004816 Published online by Cambridge University Press

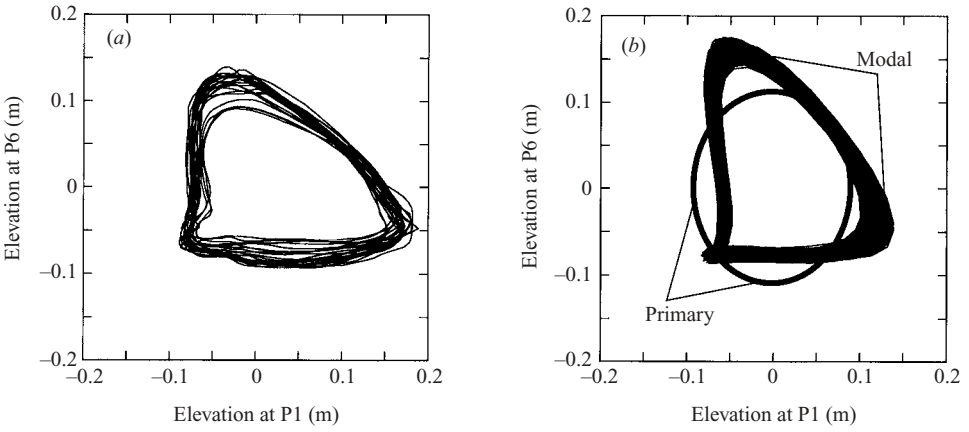


FIGURE 21. As figure 20 but for longitudinal excitation $\sigma/\sigma_1 = 1.0109$.

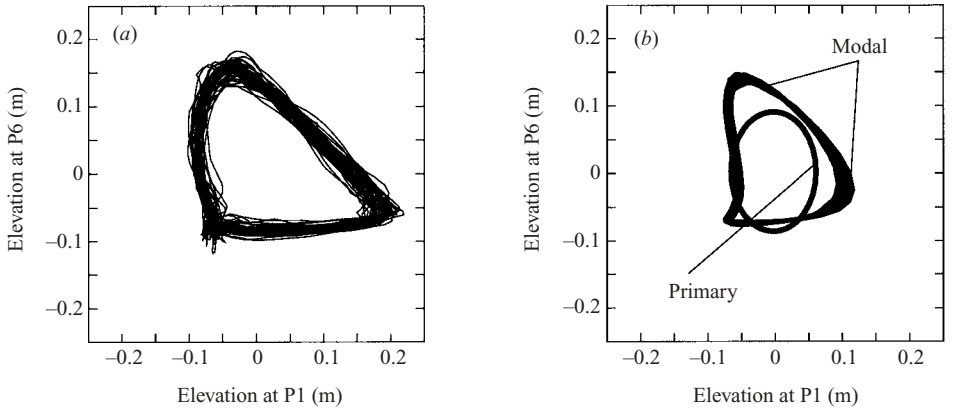


FIGURE 22. As figure 21 but with $\sigma/\sigma_1 = 0.997$.

especially true for diagonal forcing, where the maximum difference between modal theory and experiments was 9%. However, we could not obtain similar agreement with experimental data for longitudinal forcing. While the measured and calculated wave elevations at Probe 6 give a maximum 9% difference, the measured data at Probe 1 are always larger than the theoretical values. The discrepancy is largest for smaller σ. When the theory indicates minimum amplitude A for the dominant mode in 'swirling' motions, the experiment demonstrates increasing corresponding elevation near the wall. The difference reaches a maximum of 30%. A possible explanation is connected with the significant amplification of higher modes. This means that some higher modes should be considered to have the same order as the primary dominant in a similar way as done for two-dimensional sloshing by Faltinsen & Timokha (2001). Another explanation is connected with run-up phenomena near the wall, which may increase the measured data.

Our analysis of transient regimes showed that three-dimensional sloshing in the initial time range depends dramatically on the initial condition. A simple explanation of this may be made for 'swirling' modes when a small change of the initial conditions will determine the direction of wave rotation. However, for excitation frequencies in the effective domain of 'planar' and 'diagonal' waves (slightly away from primary

https://doi.org/10.1017/S0022112003004816 Published online by Cambridge University Press

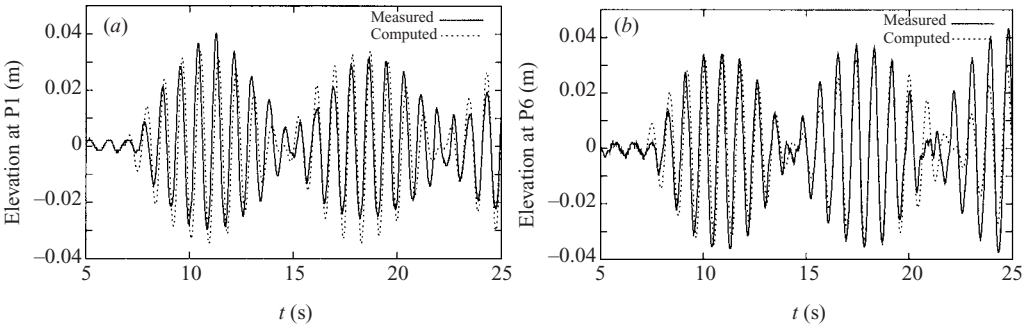


FIGURE 23. Transient waves for diagonal excitation with $h = 0.508$, $\sigma/\sigma_1 = 1.1$. (a) Comparison of measured and computed data at Probe 1, (b) comparison at Probe 6.

resonance) the computed results are not significantly affected by initial conditions. We demonstrate this for one case from the series with diagonal excitation in figure 23(a, b). Even though the experiments show initial waves (actual sinusoidal forcing starts from $t = 6.85$ s), the simulations with zero-initial conditions give good agreement with experimental data.

5. Conclusions

The adaptive third-order modal approach by Faltinsen & Timokha (2001) was modified to handle three-dimensional sloshing in a rectangular-base basin. The assumptions are incompressible fluid, irrotational flow, no overturning waves and no roof impacts. The free surface should intersect the tank walls perpendicularly. In addition, the lateral and angular external forcing is sufficiently small and characterized by the dimensionless parameter $\epsilon \ll 1$. Our modal approach derived an infinite-dimensional system of ordinary differential equations coupling nonlinearly time-dependent (modal) functions $\beta_{i,j}$ describing time-evolution of corresponding natural surface modes. The nonlinearity is of polynomial type. This is for instance consistent with the third-order theory by Zakharov (1968). The adaptive modal theory may account for amplification of an infinite number of the natural modes. Its limitations for description of local phenomena like run-up and breaking waves and comparison with Perko-like analytical schemes (La Rocca *et al.* 2000) are extensively discussed by Faltinsen & Timokha (2002*a*).

The adaptive system is simplified for sloshing in a rectangular-base basin with similar breadth and width and finite fluid depth. The simplification is based on asymptotic ordering of $\beta_{i,j}$ assuming two primary dominating modes of $O(\epsilon^{1/3})$. This ordering reduces the adaptive systems to a finite-dimensional nonlinear system for nine modal functions. The nonlinear system is completed by an infinite-dimensional linear system for the remaining modal functions. If cross-waves are not excited, it coincides with the modal system of Faltinsen *et al.* (2000) derived for two-dimensional sloshing. The two-dimensional results by Faltinsen *et al.* (2000) can be used as an indicator of the limitation of our three-dimensional model in capturing the longitudinally excited primary mode in terms of depth/breadth ratio h and forcing amplitude. If the forcing amplitude is sufficiently small, h should be larger than 0.24.

The problem of resonant sloshing in a square-base basin with excitation frequency close to the lowest natural frequency was examined. A Bubnov–Galerkin scheme

https://doi.org/10.1017/S0022112003004816 Published online by Cambridge University Press

combined with an asymptotic technique was implemented (Faltinsen *et al.* 2000) to find steady-state waves. These gave an asymptotic approximation of periodic solutions correct to $O(\epsilon)$. A secular system of nonlinear algebraic equations couples the dominant amplitudes of the primary modes. It is formally analogous to the secular system of Gavrilyuk *et al.* (2000) derived for sloshing in a circular basin due to longitudinal (surge/pitch) forcing. The response depends on the three coefficients m_i in the system, which are functions of depth and excitation frequency. The coefficients m_i are approximately constant for $h > 1$ and vary very slowly for $h_1 < h < 1$ (here h_1 is the critical depth corresponding to the change from 'hard' to 'soft' spring response of two-dimensional sloshing). Our modal system, can by introducing a slow-time scale, be used for derivation of a two-dimensional system of ordinary differential equations in a form similar to Bridges (1986) (free oscillations) and Feng & Sethna (1989) (parametric excitation) but with other forcing terms. Similar to sloshing in a circular-base tank, two steady-state responses occur in a square-base basin, namely 'planar' (in the plane of excitation) and 'swirling' (rotary motions). In addition, square geometry yields so-called 'square'-like (nearly diagonal) steady-state waves. Nearly diagonal waves were theoretically established by Bryant & Stiassnie (1995) and Bridges (1987) for free fluid oscillations. Waterhouse (1995) presented periodic solutions, which can also be interpreted as 'square'-like motions. Finally, diagonal-like waves were observed experimentally by Tomawa & Sueoka (1989) for small fluid depths. Adopting a stability analysis scheme by neglecting perturbations in non-leading modes (analogous to Faltinsen 1974; Miles 1984*a*; Bridges 1986), we were able to calculate effective frequency domains for the different wave behaviour and find critical depths where either the frequency domains of stable regimes or their wave response may change dramatically. Summarized results are presented in figure 10. For longitudinal (along the walls) excitation and $h > h_1$ there is the same qualitative structure as for resonant sloshing in a circular basin, namely the small neighbourhood of the primary resonance consists of two zones, where stable 'swirling' and irregular (no stable steady-state solutions) motions are realized. Stable 'planar' sloshing occurs for excitation frequencies slightly away from the main resonance. This zone falls into two non-connected regions, i.e. for lower and larger excitation frequencies than the primary one. The left region (for lower frequencies) contacts the frequency domain of irregular waves, while the right region partly overlaps the effective domain for 'swirling'. The effective domain for 'square'-like modes is in general overlapped by the left region of 'planar' waves. Moreover, its steady amplitude is significantly larger than the amplitude of the 'planar' waves. Therefore, experiments will most probably not capture steady-state 'square'-like waves with a static initial fluid state. The situation changes with decreasing h. The frequency domain of stable 'square'-like waves then occupies a small vicinity of the primary resonance instead of the regions of irregular waves, while the 'swirling' frequency domain moves away from the primary resonant zone. Taking into account the theoretical results by Ockendon *et al.* (1996), calculations by Wu *et al.* (1998) and experimental observations by Tomawa & Sueoka (1989) it is believed that this type of motion initializes diagonal-like wave-trains in shallow fluid sloshing.

When $h > h_1$ and the excitation is in the diagonal plane of the square base, three, and only three, independent periodic solutions were found. One of them ('diagonal') is associated with synchronous cosine-like amplification of the primary dominant modes having equal amplitudes. It occurs in the diagonal plane and is formally analogous to 'planar' waves from the longitudinal excitation case. There is also a frequency domain for stable 'swirling' modes in the vicinity of the main resonance. In addition, there

https://doi.org/10.1017/S0022112003004816 Published online by Cambridge University Press

are 'square'-like modes appearing at an angle to the excitation plane (synchronous amplification of the primary dominants with different amplitudes), but this regime is always unstable. The main difference from longitudinal excitation is that for $0.5 > h > h_1$ stable steady-state solutions exist for all excitation frequencies close to the main resonance and there is a zone where 'swirling' and 'diagonal' modes of comparable amplitude co-exist. This removes the range of 'chaotic' (no stable steady-state regimes) motions. Additional future analysis should clarify the situation for arbitrary guiding excitation vectors. There is probably a set of critical angles where the frequency domain with 'chaos' disappears.

An experimental study of resonant sloshing was conducted for longitudinal and diagonal forcing (due to horizontal tank motions) with $h = 0.508,\ 0.34$ and 0.27 and a small excitation amplitude (amplitude/breadth ratio 0.0078). Since transients did not die out even after approximately 120 excitation periods (this highlights the minor dissipation effect), some additional efforts were made to identify the measured data in terms of expected steady-state motions. The classification of experimental results was made by both visual observations and post-experimental analysis of recorded wave elevations near the tank walls. Theoretical and experimental effective frequency domains of different steady-state wave motions agreed well for both longitudinal and diagonal forcing. There were some problems in identifying which steady-state solution is realized for diagonal forcing in the frequency domain where 'swirling' and 'diagonal' sloshing of similar amplitude co-exist. Additional experimental and theoretical studies on possible waves in this frequency domain are therefore needed. The experiments should be done for longer time series and the possibility of stable non-harmonic solutions should be theoretically investigated.

A quantitative comparison of the theoretical and experimental wave elevations was also presented. The validation of steady-state regimes used direct numerical simulations with initial conditions calculated from asymptotic periodical solutions (up to $o(\epsilon)$). They agreed very well for 'planar' and 'diagonal' motions, while the calculated wave elevations near the wall for the 'swirling' mode gave maximum wave elevation amplitude up to 30% lower than in the experiments. However, the error was significantly larger when using only dominating modes (up to 200%). This confirmed implicitly that modification of the modal system should account for some higher modes having the same order of magnitude as formally dominating ones. Another source of improvements is connected with unsolved local phenomena documented by video for 'swirling' regimes. These local phenomena appeared as very steep waves with possible run-up and overturning (similar observations were reported by Arai *et al.* 1992*a* and Chen & Arai 1995). Local phenomena may significantly increase the measured values at the walls. Similar phenomena were reported by Faltinsen *et al.* (2000) and Faltinsen & Timokha (2002*a*) for two-dimensional sloshing with either intermediate depths or for sufficiently large excitation amplitude or near the critical depth $h = h_1$. A future study should also focus on a quantitative description of both transient and steady-state solutions up to $O(\epsilon)$ by direct numerical integration of our modal system. This will require experimental data on initial free-surface shapes and velocities. Preliminary calculations showed that actual three-dimensional sloshing depends strongly on small changes in initial conditions. However, initial conditions give negligible changes in the time evolution for frequency domains where 'planar' or 'diagonal' steady regimes are expected. Another future study could address resonant sloshing with small deviations between breadth and width (nonlinear free-surface waves have been investigated by Bridges 1985, 1987). Systematic studies for increasing forcing amplitude and decreasing fluid depth, including intermediate depth, should be

https://doi.org/10.1017/S0022112003004816 Published online by Cambridge University Press

done for a tank with similar length and breadth in the same way as done by Faltinsen & Timokha (2002*a*). The intermediate-depth case requires Boussinesq-type ordering and strongly multimodal structure in order to describe progressively activated modes. A further problem is to estimate dissipative effects during sloshing, especially for intermediate and shallow depths when they have a dominating character.

A.N.T. is grateful for support from Anders Jahre's Foundation for Advancement of Science.

Appendix A. Derivation of the asymptotic modal system

Prior to beginning the derivation we need to define some auxiliary tensors. These are $\Lambda^{(N-2)}_{\underbrace{i\dots m}_{N}}$ defined by the integrals

$$\Lambda^{(0)}_{ij}=\int_{-1/2}^{1/2} f^{(1)}_i f^{(1)}_j\,\mathrm{d}x=\begin{cases}1, & i=j=0\\ \frac{1}{2}, & i=j\neq 0,\\ 0, & i\neq j,\end{cases}$$

$$\Lambda^{(1)}_{i,j,k}=\int_{-1/2}^{1/2} f^{(1)}_i f^{(1)}_j f^{(1)}_k\,\mathrm{d}x=\tfrac{1}{2}\left(\Lambda^{(0)}_{|j-i|k}+\Lambda^{(0)}_{|i+j|k}\right),$$

$$\dots\dots\dots

In a similar way

$$\int_{-1/2r}^{1/2r} \left(f_n^{(2)}\right)' \left(f_m^{(2)}\right)' \underbrace{f_i^{(2)} \dots f_k^{(2)}}_{N} \,\mathrm{d}y = r\,\Lambda_{nm,i\dots k}^{(-N)}.$$

Simple calculation shows that

$$\frac{\partial A_{n,k}}{\partial \beta_{i,j}} = \int_{-1/2}^{1/2} \int_{-1/2r}^{1/2r} \varphi_{n,k}(x, y, f) f_i^{(1)} f_j^{(1)} \,\mathrm{d}y \,\mathrm{d}x. \tag{A 1}$$

Here $\varphi_{n,k}(x, y, f)$ should include terms up to $O(\beta^2) = O(\epsilon^{2/3})$, namely $\varphi_{n,k} \approx \varphi_{n,k}(x, y, 0) + (\partial \varphi_{n,k}/\partial z) f + \frac{1}{2}(\partial^2 \varphi_{n,k}/\partial z^2) f^2$. This gives

$$\begin{aligned}\varphi_{n,k}(x, y, f) = f_n^{(1)} f_k^{(2)} + E_{n,k}\left(f_n^{(1)} f_p^{(1)}\right)\left(f_k^{(2)} f_q^{(2)}\right)\beta^{p,q} \\ + D_{n,k}\left(f_n^{(1)} f_p^{(1)} f_l^{(1)}\right)\left(f_k^{(2)} f_q^{(2)} f_m^{(2)}\right)\beta^{p,q}\beta^{l,m},\end{aligned} \tag{A 2}$$

where $E_{n,k} = \lambda_{n,k} \tanh(\lambda_{n,k} h)$, $D_{n,k} = \lambda_{n,k}^2/2$.

Setting (A 2) into (A 1) leads to the following expressions:

$$\frac{\partial A_{n,k}}{\partial \beta_{i,j}} = \frac{1}{r}\left(\Lambda_{ni}^{(0)} \Lambda_{kj}^{(0)} + E_{n,k} \Lambda_{npi}^{(1)} \Lambda_{kqj}^{(1)} \beta^{p,q} + D_{n,k} \Lambda_{npli}^{(2)} \Lambda_{kqmj}^{(2)} \beta^{p,q} \beta^{l,m}\right).$$

Processing in a similar way we obtain $A_{(n,k)(i,j)}$ correct to $O(\beta^2)$:

$$\begin{aligned} A_{(n,k)(i,j)} &= \Pi_{(n,k)(i,j)}^{(0)} + \beta^{p,q} \Pi_{(n,k)(i,j),(p,q)}^{(1)} + \beta^{p,q}\beta^{a,b} \Pi_{(n,k)(i,j),(p,q)(a,b)}^{(2)}, \\ \frac{\partial A_{(n,k),(i,j)}}{\partial \beta_{l,m}} &= \Pi_{(n,k)(i,j),(l,m)}^{(1)} + 2\beta^{p,q} \Pi_{(n,k)(i,j),(l,m)(p,q)}^{(2)}, \end{aligned}$$

where

$$\Pi_{(n,k)(i,j)}^{(0)} = \frac{E_{n,k}}{r} \Lambda_{ni}^{(0)} \Lambda_{kj}^{(0)},$$

$$\Pi_{(n,k)(i,j),(p,q)}^{(1)} = \frac{\Lambda_{ni,p}^{(-1)} \Lambda_{kjq}^{(1)}}{r} + r\,\Lambda_{kj,q}^{(-1)} \Lambda_{nip}^{(1)} + \frac{1}{r} E_{n,k} E_{i,j} \Lambda_{nip}^{(1)} \Lambda_{kjq}^{(1)},$$

$$\begin{aligned}\Pi_{(n,k)(i,j),(p,q)(a,b)}^{(2)} = \left(\frac{\Lambda_{ni,ap}^{(-2)} \Lambda_{kj,bq}^{(2)}}{r} + r\,\Lambda_{kj,bq}^{(-2)} \Lambda_{niap}^{(2)}\right) \frac{E_{n,k} + E_{i,j}}{2} \\ + \frac{1}{r} \Lambda_{niap}^{(2)} \Lambda_{kjbq}^{(2)} (D_{n,k} E_{i,j} + D_{i,j} E_{n,k}).\end{aligned}$$

Considering (2.11) as a linear algebraic equation relative to $R^{i,j}$ suggests the following asymptotic solution:

$$R^{i,j} = V_{(a,b)}^{1,(i,j)} \dot{\beta}^{(a,b)} + V_{(a,b),(c,d)}^{2,(i,j)} \dot{\beta}^{a,b} \beta^{c,d} + \bar{V}_{(a,b),(c,d)(e,f)}^{3,(i,j)} \dot{\beta}^{a,b} \beta^{c,d} \beta^{e,f}. \tag{A 3}$$

Substituting (A 3) into (2.11) and collecting terms in $\dot{\beta}_{i,j}$ and $\beta_{i,j}$ up to third polynomial order gives

$$V_{(a,b)}^{1,(n,k)} = \frac{\delta_{an}\delta_{kb}}{E_{n,k}},$$

$$V_{(a,b),(c,d)}^{2,(n,k)} = \left[\frac{E_{n,k} \Lambda_{nca}^{(1)} \Lambda_{kdb}^{(1)}}{r} - \frac{\Pi_{(n,k)(a,b),(c,d)}^{(1)}}{E_{a,b}}\right] \Bigg/ \left(\frac{E_{n,k} \Lambda_{nn}^{(0)} \Lambda_{kk}^{(0)}}{r}\right),$$

https://doi.org/10.1017/S0022112003004816 Published online by Cambridge University Press

$$V^{3,(n,k)}_{(a,b),(c,d),(e,f)} = \left[\frac{D_{n,k}\Lambda^{(2)}_{ncea}\Lambda^{(2)}_{kdfb}}{r} - \frac{\Pi^{(2)}_{(n,k)(a,b),(c,d)(e,f)}}{E_{a,b}} - \Pi^{(1)}_{(n,k)(i,j),(e,f)}V^{2,(i,j)}_{(a,b),(c,d)}\right] \Bigg/ \left(\frac{E_{n,k}\Lambda^{(0)}_{nn}\Lambda^{(0)}_{kk}}{r}\right),$$

$$\bar{V}^{3,(n,k)}_{(a,b),(c,d)(e,f)} = \frac{1}{2}\left[V^{3,(n,k)}_{(a,b),(c,d),(e,f)} + V^{3,(n,k)}_{(a,b),(e,f),(c,d)}\right],$$

where δ_{ij} is the Kronecker symbol.

Simple calculations give

$$\frac{\partial l_1}{\partial \beta_{i,j}} = \frac{\delta_{0j}}{r(\pi i)^2}[(-1)^i - 1], \quad \frac{\partial l_2}{\partial \beta_{i,j}} = \frac{\delta_{0i}}{r^2(\pi j)^2}[(-1)^j - 1], \quad \frac{\partial l_3}{\partial \beta_{i,j}} = \frac{\Lambda^{(0)}_{ii}\Lambda^{(0)}_{jj}}{r}\beta_{i,j}.$$

Calculations of $l_{k\omega}$ and $l_{k\omega t}$ are much more complicated. An asymptotic solution of the Stokes–Zhukovsky potentials (Ω_1- and Ω_2-scalar harmonic components) is needed from the following Neumann boundary value conditions:

$$\left.\frac{\partial \Omega_1}{\partial x}\right|_{x=\pm\frac{1}{2}} = 0, \quad \left.\frac{\partial \Omega_1}{\partial y}\right|_{y=\pm\frac{1}{2r}} = -z, \quad \left.\frac{\partial \Omega_1}{\partial z}\right|_{z=-h} = y, \quad \left.\frac{\partial \Omega_1}{\partial \nu}\right|_{z=f} = \frac{y + ff_y}{\sqrt{1 + f_x^2 + f_y^2}},$$

$$\left.\frac{\partial \Omega_2}{\partial x}\right|_{x=\pm\frac{1}{2}} = z, \quad \left.\frac{\partial \Omega_1}{\partial y}\right|_{y=\pm\frac{1}{2r}} = 0, \quad \left.\frac{\partial \Omega_1}{\partial z}\right|_{z=-h} = -x, \quad \left.\frac{\partial \Omega_1}{\partial \nu}\right|_{z=f} = -\frac{x + ff_x}{\sqrt{1 + f_x^2 + f_y^2}}.$$

Since $\omega_i = O(\epsilon)$, $i = 1, 2$ the required asymptotic components $\partial l_{k\omega}/\partial\beta_{i,j}$ and $\partial l_{k\omega t}/\partial\beta_{i,j}$ should be expressed correctly to $O(1)$. This implies that $l_{k\omega}$, $l_{k\omega t}$ and Ω_k should contain only linear terms in $\beta_{i,j}$. The procedure gives

$$\left.\begin{aligned}\Omega_1 &= \Omega_0^{(1)}(y,z) + \chi^{1,(i,j)}(t) f_i^{(1)} f_j^{(2)} \tfrac{\cosh(\lambda_{i,j}(z+h))}{\cosh(\lambda_{i,j}h)} + o(\beta),\\ \Omega_2 &= \Omega_0^{(2)}(x,z) + \chi^{2,(i,j)}(t) f_i^{(1)} f_j^{(2)} \tfrac{\cosh(\lambda_{i,j}(z+h))}{\cosh(\lambda_{i,j}h)} + o(\beta),\end{aligned}\right\} \tag{A 4}$$

where $\chi^{k,(i,j)}$ are linear combinations in $\beta_{i,j}$. $\Omega_0^{(k)}$ are two-dimensional solutions of the Neumann boundary value problems

$$\Delta\Omega_0^{(1)} = 0 \quad \left(-\frac{1}{2r} < y < \frac{1}{2r}, \ -h < z < 0\right), \quad \left.\frac{\partial \Omega_0^{(1)}}{\partial z}\right|_{z=0,-h} = y, \quad \left.\frac{\partial \Omega_0^{(1)}}{\partial y}\right|_{y=\pm 1/2r} = -z,$$

$$\Delta\Omega_0^{(2)} = 0 \quad \left(-\frac{1}{2} < x < \frac{1}{2}, \ -h < z < 0\right), \quad \left.\frac{\partial \Omega_0^{(2)}}{\partial z}\right|_{z=0,-h} = -x, \quad \left.\frac{\partial \Omega_0^{(2)}}{\partial x}\right|_{x=\pm 1/2} = z.$$

The solutions according to Faltinsen *et al.* (2000) are

$$\Omega_0^{(1)} = -yz + 2a^{1,i} f_i^{(2)}(y)\frac{\sinh(\pi r i(z + \frac{1}{2}h))}{\cosh(\pi r i h/2)}, \quad \Omega_0^{(2)} = xz - 2a^{2,i} f_i^{(1)}(x)\frac{\sinh(\pi i(z + \frac{1}{2}h))}{\cosh(\pi i h/2)},$$

where

$$a^{1,i} = \frac{2}{r^2(i\pi)^3}[(-1)^i - 1], \quad a^{2,i} = \frac{2}{(i\pi)^3}[(-1)^i - 1].$$

Inserting (A 4) into expressions for $l_{k\omega}$ and $l_{k\omega t}$ gives

$$\frac{\partial l_{k\omega t}}{\partial \beta_{i,j}} = O(\beta), \quad \frac{\partial l_{k\omega}}{\partial \beta_{i,j}} = \int_{-1/2}^{1/2}\int_{-1/2r}^{1/2r} \Omega_0^{(k)}\Big|_{z=0} f_i^{(1)} f_j^{(2)}\,\mathrm{d}y\,\mathrm{d}x + o(\beta),$$

https://doi.org/10.1017/S0022112003004816 Published online by Cambridge University Press

where the last expression becomes zero unless either $i = 0,\ k = 1$ or $j = 0,\ k = 2$, namely

$$\frac{\partial l_{2\omega}}{\partial \beta_{i,j}} = -\frac{2\delta_{0j}}{r(i\pi)^3}[(-1)^i - 1]\tanh(\pi i h/2), \qquad \frac{\partial l_{1\omega}}{\partial \beta_{i,j}} = \frac{2\delta_{i0}}{r^2(j\pi)^3}[(-1)^j - 1]\tanh(\pi r j h/2).$$

Projections of the gravitational acceleration vector onto the $Oxyz$-axes depend on instantaneous angular position $\psi_i,\ i = 1, 2$:

$$g_1 = g\psi_2(t) + o(\epsilon), \quad g_2 = -g\psi_1(t) + o(\epsilon), \quad g_3 = -g + o(\epsilon).$$

This completes the calculations of the forcing terms as follows:

$$\frac{\delta_{0i}}{r^2(\pi j)^2}[(-1)^j - 1]\left[\dot{v}_{O2} + S_j^{(2)}\ddot{\psi}_1 + g\psi_1\right] + \frac{\delta_{0j}}{r(\pi i)^2}[(-1)^i - 1]\left[\dot{v}_{O1} - S_i^{(1)}\ddot{\psi}_2 - g\psi_2\right],$$

where

$$S_i^{(1)} = \frac{2}{\pi i}\tanh(\pi i h/2), \quad S_j^{(2)} = \frac{2}{\pi j}\tanh(\pi r j h/2). \tag{A 5}$$

After collecting all the components we arrive at the asymptotic modal system (2.15), where

$$P_{i,j}^{(1)} = \frac{2\delta_{0j}E_{i,0}}{(\pi i)^2}[(-1)^i - 1], \quad P_{i,j}^{(2)} = \frac{2\delta_{0i}E_{0,j}}{r(\pi j)^2}[(-1)^j - 1]. \tag{A 6}$$

We have the following coefficients defined in (2.15):

$$d^{1,(i,j)}_{(a,b),(c,d)} = E^{i,j}V^{2,(i,j)}_{(a,b),(c,d)} + E_{i,j}\frac{\Lambda^{(1)}_{aci}\Lambda^{(1)}_{bdj}}{\Lambda^{(0)}_{ii}\Lambda^{(0)}_{jj}},$$

$$d^{2,(i,j)}_{(a,b),(c,d),(e,f)} = E^{i,j}\bar{V}^{3,(i,j)}_{(a,b),(c,d)(e,f)} + \frac{E_{n,k}E_{i,j}\Lambda^{(1)}_{nei}\Lambda^{(1)}_{kfj}V^{2,(n,k)}_{(a,b),(c,d)}}{\Lambda^{(0)}_{ii}\Lambda^{(0)}_{jj}} + \frac{D_{a,b}E_{i,j}\Lambda^{(2)}_{acei}\Lambda^{(2)}_{bdfj}}{E_{a,b}\Lambda^{(0)}_{ii}\Lambda^{(0)}_{jj}},$$

$$t^{0,(i,j)}_{(a,b),(c,d)} = E^{i,j}V^{2,(i,j)}_{(a,b),(c,d)} + \frac{rE_{i,j}\Pi^{(1)}_{(a,b)(c,d),(i,j)}}{2E_{a,b}E_{c,d}\Lambda^{(0)}_{ii}\Lambda^{(0)}_{jj}},$$

$$t^{1,(i,j)}_{(a,b),(c,d),(e,f)} = 2E^{i,j}\bar{V}^{3,(i,j)}_{(a,b),(c,d)(e,f)} + \frac{E_{i,j}E_{n,k}\Lambda^{(1)}_{nei}\Lambda^{(1)}_{kfj}V^{2,(n,k)}_{(a,b),(c,d)}}{\Lambda^{(0)}_{ii}\Lambda^{(0)}_{jj}} + \frac{rE_{i,j}\Pi^{(2)}_{(a,b)(c,d),(i,j)(e,f)}}{E_{a,b}E_{c,d}\Lambda^{(0)}_{ii}\Lambda^{(0)}_{jj}}$$
$$+ \frac{rE_{i,j}V^{2,(n,k)}_{(a,b),(e,f)}\Pi^{(1)}_{(n,k)(c,d),(i,j)}}{2E_{c,d}\Lambda^{(0)}_{ii}\Lambda^{(0)}_{jj}} + \frac{rE_{i,j}V^{2,(n,k)}_{(c,d),(e,f)}\Pi^{(1)}_{(n,k)(a,b),(i,j)}}{2E_{a,b}\Lambda^{(0)}_{ii}\Lambda^{(0)}_{jj}}.$$

Appendix B. Coefficients for the asymptotic modal system (3.3)

$$d_1 = d^{1,(1,0)}_{(1,0),(2,0)} = t^{0,(1,0)}_{(1,0),(2,0)} + t^{0,(1,0)}_{(2,0),(1,0)}, \quad d_2 = d^{2,(1,0)}_{(1,0),(1,0),(1,0)} = t^{1,(1,0)}_{(1,0),(1,0),(1,0)},$$
$$d_3 = d^{1,(1,0)}_{(2,0),(1,0)}, \quad d_4 = d^{1,(2,0)}_{(1,0),(1,0)}, \quad d_5 = t^{0,(2,0)}_{(1,0),(1,0)},$$
$$d_6 = d^{2,(1,0)}_{(1,0),(0,1),(0,1)}, \quad d_7 = d^{1,(1,0)}_{(0,1),(1,1)}, \quad d_8 = d^{2,(1,0)}_{(0,1),(0,1),(1,0)} + d^{2,(1,0)}_{(0,1),(1,0),(0,1)},$$
$$d_9 = d^{1,(1,0)}_{(1,1),(0,1)}, \quad d_{10} = t^{1,(1,0)}_{(0,1),(0,1),(1,0)}, \quad d_{11} = t^{1,(1,0)}_{(1,0),(0,1),(0,1)} + t^{1,(1,0)}_{(0,1),(1,0),(0,1)},$$

https://doi.org/10.1017/S0022112003004816 Published online by Cambridge University Press

$$d_{12} = t^{0,(1,0)}_{(0,1),(1,1)} + t^{0,(1,0)}_{(1,1),(0,1)};$$

$$\bar{d}_1 = d^{1,(0,1)}_{(0,1),(0,2)} = t^{0,(0,1)}_{(0,1),(0,2)} + t^{0,(0,1)}_{(0,2),(0,1)}, \quad \bar{d}_2 = d^{2,(0,1)}_{(0,1),(0,1),(0,1)} = t^{1,(0,1)}_{(0,1),(0,1),(0,1)}.$$

$$\bar{d}_3 = d^{1,(0,1)}_{(0,2),(0,1)}, \quad \bar{d}_4 = d^{1,(0,2)}_{(0,1),(0,1)}, \quad \bar{d}_5 = t^{0,(0,2)}_{(0,1),(0,1)},$$

$$\bar{d}_6 = d^{2,(0,1)}_{(0,1),(1,0),(1,0)}, \quad \bar{d}_7 = d^{1,(0,1)}_{(1,0),(1,1)}, \quad \bar{d}_8 = d^{2,(0,1)}_{(1,0),(1,0),(0,1)} + d^{2,(0,1)}_{(1,0),(0,1),(1,0)},$$

$$\bar{d}_9 = d^{1,(0,1)}_{(1,1),(1,0)}, \quad \bar{d}_{10} = t^{1,(0,1)}_{(1,0),(1,0),(0,1)}, \quad \bar{d}_{11} = t^{1,(0,1)}_{(1,0),(0,1),(1,0)} + t^{1,(0,1)}_{(0,1),(1,0),(1,0)},$$

$$\bar{d}_{12} = t^{0,(0,1)}_{(1,0),(1,1)} + t^{0,(0,1)}_{(1,1),(1,0)};$$

$$\hat{d}_1 = d^{1,(1,1)}_{(1,0),(0,1)}, \quad \hat{d}_2 = d^{1,(1,1)}_{(0,1),(1,0)}, \quad \hat{d}_3 = t^{0,(1,1)}_{(1,0),(0,1)} + t^{0,(1,1)}_{(0,1),(1,0)};$$

$$q_1 = d^{1,(3,0)}_{(1,0),(2,0)}, \quad q_1 = d^{2,(3,0)}_{(1,0),(1,0),(1,0)}, \quad q_3 = d^{1,(3,0)}_{(2,0),(1,0)}, \quad q_4 = t^{1,(3,0)}_{(1,0),(1,0),(1,0)},$$

$$q_5 = t^{0,(3,0)}_{(1,0),(2,0)} + t^{0,(3,0)}_{(2,0),(1,0)}, \quad q_6 = d^{1,(2,1)}_{(1,0),(1,1)}, \quad q_7 = d^{2,(2,1)}_{(1,0),(1,0),(0,1)} + d^{2,(2,1)}_{(1,0),(0,1),(1,0)},$$

$$q_8 = d^{1,(2,1)}_{(0,1),(2,0)}, \quad q_9 = d^{2,(2,1)}_{(0,1),(0,1),(1,0)}, \quad q_{10} = d^{1,(2,1)}_{(2,0),(0,1)}, \quad q_{11} = d^{1,(2,1)}_{(1,1),(1,0)},$$

$$q_{12} = t^{1,(2,1)}_{(1,0),(1,0),(0,1)}, \quad q_{13} = t^{1,(2,1)}_{(1,0),(0,1),(1,0)} + t^{1,(2,1)}_{(0,1),(1,0),(1,0)},$$

$$q_{14} = t^{0,(2,1)}_{(1,0),(1,1)} + t^{0,(2,1)}_{(1,1),(1,0)}, \quad q_{15} = t^{0,(2,1)}_{(0,1),(2,0)} + t^{0,(2,1)}_{(2,0),(0,1)},$$

$$\bar{q}_1 = d^{1,(0,3)}_{(0,1),(0,2)}, \quad \bar{q}_2 = d^{2,(0,3)}_{(0,1),(0,1),(0,1)}, \quad \bar{q}_3 = d^{1,(0,3)}_{(0,2),(0,1)}, \quad \bar{q}_4 = t^{1,(0,3)}_{(0,1),(0,1),(0,1)},$$

$$\bar{q}_5 = t^{0,(0,3)}_{(0,1),(0,2)} + t^{0,(0,3)}_{(0,2),(0,1)}, \quad \bar{q}_6 = d^{1,(1,2)}_{(0,1),(1,1)}, \quad \bar{q}_7 = d^{2,(1,2)}_{(0,1),(0,1),(1,0)} + d^{2,(1,2)}_{(0,1),(1,0),(0,1)}.$$

$$\bar{q}_8 = d^{1,(1,2)}_{(1,0),(0,2)}, \quad \bar{q}_9 = d^{2,(1,2)}_{(1,0),(0,1),(0,1)}, \quad \bar{q}_{10} = d^{1,(1,2)}_{(0,2),(1,0)}, \quad \bar{q}_{11} = d^{1,(1,2)}_{(1,1),(0,1)},$$

$$\bar{q}_{12} = t^{1,(1,2)}_{(0,1),(0,1),(1,0)}, \quad \bar{q}_{13} = t^{1,(1,2)}_{(1,0),(0,1),(0,1)} + t^{1,(1,2)}_{(0,1),(1,0),(0,1)},$$

$$\bar{q}_{14} = t^{0,(1,2)}_{(0,1),(1,1)} + t^{0,(1,2)}_{(1,1),(0,1)}, \quad \bar{q}_{15} = t^{0,(1,2)}_{(1,0),(0,2)} + t^{0,(1,2)}_{(0,2),(1,0)}.$$

REFERENCES

Abramson, H. N. 1966 The dynamics of liquids in moving containers. *NASA Rep.* SP 106.

Abramson, H. N., Bass, R. L., Faltinsen, O. M. & Olsen, H. A. 1974 Liquid slosh in LNG Carriers. In *Tenth Symp. on Naval Hydrodynamics, June 24–28, 1974, Cambridge, Massachusetts.* ACR-204, pp. 371–388.

Aliabadi, S., Johnson, A. & Abedi, J. 2003 Comparison of finite element and pendulum models for simulation of sloshing. *Computers Fluids.* **23**, 535–545.

Arai, M., Cheng, L. Y. & Inoue, Y. 1992*a* 3D numerical simulation of impact load due to liquid cargo sloshing. *J. Soc. Nav. Arch. Japan.* **171**, 177–185.

Arai, M., Cheng, L. Y. & Inoue, Y. 1993 Numerical simulation of sloshing and swirling in cubic and cylindrical tank. *J. Kansai Soc. Nav. Arch. Japan.* **219**, 97–101.

Arai, M., Cheng, L. Y., Inoue, Y., Sasaki, H. & Yamagishi, N. 1992*b* Numerical analysis of liquid sloshing in tanks of FPSO. *Proc. Second (1992) Intl Offshore and Polar Conf., San Francisco, USA, 14–19 June 1992*, vol. 3, 383–390.

Bader, G. & Ascher, U. 1987 A new basis implementation for a mixed order boundary value ODE solver. *SIAM J. Sci. Statist. Comput.* **8**, 483–500.

Bridges, T. J. 1985 On secondary bifurcation of three dimensional standing waves. *Tech. Summary Rep. Wisconsin Univ., Madison.*

Bridges, T. J. 1986 On secondary bifurcation of three-dimensional standing waves. *SIAM J. Appl. Maths* **47**, 40–59.

Bridges, T. J. 1987 Secondary bifurcation and change of type for three dimensional standing waves in finite depth. *J. Fluid Mech.* **179**, 137–153.

https://doi.org/10.1017/S0022112003004816 Published online by Cambridge University Press

Bridges, T. J. 1988 Strong internal resonance, $Z_1 \oplus Z_2$ symmetry, and multiple periodic solutions. *SIAM J. Math. Anal.* **19**, 1015–1031.

Bryant, P. J. 1989 Nonlinear progressive waves in a circular basin. *J. Fluid Mech.* **205**, 453–467.

Bryant, P. J. & Stiassnie, M. 1994 Different forms for nonlinear standing waves in deep water. *J. Fluid Mech.* **272**, 135–156.

Bryant, P. J. & Stiassnie, M. 1995 Water waves in a deep square basin. *J. Fluid Mech.* **302**, 65–90.

Celebi, S. M. & Akyildiz, H. 2002 Nonlinear modelling of liquid sloshing in a moving rectangular tank. *Ocean Engng* **29**, 1527–1553.

Chen, L. Y. & Arai, M. 1995 Liquid sloshing in a cubic and a cylindrical tank. *Ninth Technical Exchange and Advisory Meeting, July 24–27, 1995, Hiroshima, Japan.*

Faltinsen, O. M. 1974 A nonlinear theory of sloshing in rectangular tanks. *J. Ship. Res.* **18**, 224–241.

Faltinsen, O. M. & Rognebakke, O. F. 2000 Sloshing. *Keynote lecture. NAV 2000. Proc. Intl Conf. on Ship and Shipping Research, Venice, 19–22 September, 2000, Italy.*

Faltinsen, O. M., Rognebakke, O. F., Lukovsky, I. A. & Timokha, A. N. 2000 Multidimensional modal analysis of nonlinear sloshing in a rectangular tank with finite water depth. *J. Fluid Mech.* **407**, 201–234.

Faltinsen, O. M. & Timokha, A. N. 2001 Adaptive multimodal approach to nonlinear sloshing in a rectangular rank. *J. Fluid Mech.* **432**, 167–200.

Faltinsen, O. M. & Timokha, A. N. 2002*a* Asymptotic modal approximation of nonlinear resonant sloshing in a rectangular tank with small fluid depth. *J. Fluid Mech.* **470**, 319–357.

Faltinsen, O. M. & Timokha, A. N. 2002*b* Analytically-oriented approaches to two-dimensional fluid sloshing in a rectangular tank (survey). *Proc. Insti. Maths Ukrainian Natl. Acad. Sci. "Problems of Analytical Mechanics and its Applications"* **44**, 321–345.

Feng, Z. C. & Senthna, P. R. 1989 Symmetry-breaking bifurcations in resonant surface waves. *J. Fluid Mech.* **199**, 495–518.

Fultz, D. 1962 An experimental note on finite-amplitude standing gravity waves. *J. Fluid Mech.* **13**, 193–212.

Gavrilyuk, I., Lukovsky, I. A. & Timokha, A. N. 2000 A multimodal approach to nonlinear sloshing in a circular cylindrical tank. *Hybrid Meth. Engng* **2**, 463–483.

Henderson, D. M. & Miles, J. W. 1990 Single-mode Faraday waves in small cylinder. *J. Fluid Mech.* **213**, 95–109.

Hermann, M. & Ullrich, K. 1992 RWPKV: a software package for continuation and bifurcation problems in two-point boundary value problems. *Appl. Math. Lett.* **5**, 57–61.

Ibrahim, R. A., Pilipchuk, V. N. & Ikeda, T. 2001 Recent advances in liquid sloshing dynamics. *Appl. Mech. Res.* **54**(2), 133–199.

ISSC 1997 Report of Committee I.2 "Loads". In *Proc. 13th Intl Ship and Offshore Structures Congress* (ed. T. Moan & S. Berge) Vol. 1, pp. 59–122. Pergamon.

La Rocca, M., Mele, P. & Armenio, V. 1997 Variational approach to the problem of sloshing in a moving container. *J. Theor. Appl. Fluid Mech.* **1**(4), 280–310.

La Rocca, M., Sciortino, G. & Boniforti, M. A. 2000 A fully nonlinear model for sloshing in a rotating container. *Fluid Dyn. Res.* **27**, 23–52.

Lukovsky, I. A. 1990 *Introduction to Nonlinear Dynamics of a Solid Body with a Cavity Including a Liquid*. Kiev: Naukova dumka (in Russian).

Mikishev, G. I. 1978 *Experimental Methods in the Dynamics of Spacecraft*. Moscow: Mashinostroenie (in Russian).

Miles, J. W. 1984*a* Internally resonant surface waves in circular cylinder. *J. Fluid Mech.* **149**, 1–14.

Miles, J. W. 1984*b* Resonantly forces surface waves in circular cylinder. *J. Fluid Mech.* **149**, 15–31.

Miles, J. W. 1994 Faraday waves: rolls versus squares. *J. Fluid Mech.* **269**, 353–371.

Moiseyev, N. N. & Rumyantsev, V. V. 1968 *Dynamic Stability of Bodies Containing Fluid*. Springer.

Nagata, M. 1991 Chaotic behaviour of parametrically excited surface waves in square geometry. *Eur. J. Mech.* B/*Fluids.* **10**, 61–66.

Narimanov, G. S. 1957 Movement of a tank partly filled by a fluid: the taking into account of non-smallness of amplitude. *Prikl. Mat. Mekh.* **21**, 513–524 (in Russian).

Narimanov, G. S., Dokuchaev, L. V. & Lukovsky, I. A. 1977 *Nonlinear Dynamics of Flying Apparatus with Liquid*. Moscow: Mashinostroenie (in Russian).

https://doi.org/10.1017/S0022112003004816 Published online by Cambridge University Press

Nevolin, V. G. 1984 Parametric excitation of surface waves (survey). *Inzhenerno-phys. Z.* **47**, 1028–1042 (in Russian).

Ockendon, J. R. & Ockendon, H. 1973 Resonant surface waves. *J. Fluid Mech.* **59**, 397–413.

Ockendon, H., Ockendon, J. R. & Waterhouse, D. D. 1996 Multi-mode resonance in fluids. *J. Fluid Mech.* **315**, 317–344.

Perlin, M. & Schultz, W. W. 2000 Capillary effects on surface waves. *Annu. Rev. Fluid Mech.* **32**, 241–274.

Rognebakke, O. F. & Faltinsen, O. M. 2003 Coupling of sloshing and ship motions. *J. Ship Res.* (in press).

Royon, A., Gaudin, E., Cavellier, A. & Hopfinger, E. J. 2002 Sloshing and drop formation conditions in cylindrical liquid propellant tanks. *4th Intl Conf. on Launcher Technology "Space Launcher Liquid Propulsion", Liege, Belgium, 3–6 December, 2002.* Abstracts.

Sames, P. C., Marcouly, D. & Schellin, T. 2002 Sloshing in rectangular and cylindrical tank. *J. Ship Res.* **46**, 186–200.

Shankar, P. N. & Kidambi, R. 2002 A modal method for finite amplitude, nonlinear sloshing. *Pramana – J. Phy.* **59**, 631–651.

Simonelli, F. & Gollub, J. P. 1989 Surface wave mode interaction: effects of symmetry and degeneracy. *J. Fluid Mech.* **199**, 471–494.

Solaas, F. 1995 Analytical and numerical studies of sloshing in tanks. PhD Thesis, The Norwegian Institute of Technology, Faculty of Marine Technology, Trondheim.

Stolbetsov, V. I. 1967 On oscillations of a fluid in the tank having the shape of rectangular parallelepiped. *Mech. Zhid. i Gaza (Fluid Dyn.)* N 1, 67–76 (in Russian).

Tomawa, S. & Sueoka, H. 1989 Experimental and numerical studies on sloshing in partially filled tank. *Proc. Fourth Intl Symp. on Practical Design of Ships and Mobile Units*, pp. 57.1–57.8.

Tsai, W.-T., Yue, D. K.-P. & Yip, K. M. K. 1990 Resonantly excited regular and chaotic motions in a rectangular wave tank. *J. Fluid Mech.* **216**, 343–380.

Waterhouse, D. D. 1994 Resonant sloshing near a critical depth. *J. Fluid Mech.* **281**, 313–318.

Waterhouse, D. D. 1995 Resonant oscillations of gases and liquids in three dimensions. DPhil thesis, Oxford University.

Wu, G. X., Ma, Q. W. & Taylor, R. E. 1998 Numerical simulation of sloshing waves in 3D tank based on a finite element method. *Appl. Ocean Res.* **20**, 337–355.

Zakharov, V. E. 1968 Stability of periodic waves of finite amplitude on the surface of a deep fluid. *J. Appl. Mech. Tech. Phys.* **2**, 190–194.

https://doi.org/10.1017/S0022112003004816 Published online by Cambridge University Press